Renewable and Sustainable Energy Reviews 79 (2017) 1050–1077

Contents lists available at ScienceDirect

Renewable and Sustainable Energy Reviews

journal homepage: www.elsevier.com/locate/rser

Solar energy absorption mediated by surface plasma polaritons in spectrally selective dielectric-metal-dielectric coatings: A critical review

Atasi Dan[a], Harish C. Barshilia[b,*], Kamanio Chattopadhyay[c,d], Bikramjit Basu[a,c,**]

[a] Materials Research Centre, Indian Institute of Science, Bangalore 560012, India
[b] Nanomaterials Research Laboratory, Surface Engineering Division, CSIR-National Aerospace Laboratories, HAL Airport Road, Kodihalli, Bangalore 560017, India
[c] Interdisciplinary Centre for Energy Research, Indian Institute of Science, Bangalore 560012, India
[d] Materials Engineering, Indian Institute of Science, Bangalore 560012, India

ARTICLE INFO

Keywords:
Solar energy
Concentrating solar power
Solar selective absorber coating
Surface plasma polaritons
Dielectric-metal-dielectric stack

ABSTRACT

The effective use of solar energy has become significantly important due to unnatural weather changes and fossil fuel exhaustion. Concentrating Solar Power (CSP) technology is a promising approach to harvest solar energy in the form of heat using solar selective absorber coating. These coatings are expected to absorb maximum incoming solar radiation ($\alpha \geq 0.95$) and prevent loss of the absorbed energy as infrared radiation ($\varepsilon \leq 0.05$). Efficiency of the absorber coating can be evaluated by a metric called "Solar selectivity (α/ε)". In recent years, a number of attempts have been made to achieve remarkable selective property and high temperature stability of the absorber coating using the concept of Surface Plasma Polaritons (SPPs). The SPPs have the capability to capture solar energy by confining electromagnetic field at the metal-dielectric interface. Solar absorption, can be maximized by tailoring the optical constants of the metal and dielectric. In this review, we have described different types of solar absorber coatings with particular emphasis on dielectric-metal-dielectric (DMD) -based absorber coatings. We have presented a brief theoretical overview to comprehend physics of DMD coatings. This review additionally highlights some of the case studies based on the DMD -based absorber coatings with the high temperature stability and their importance in the context of CSP technologies.

1. Introduction

It is widely accepted that the use of fossil fuels like petroleum, natural gas and coal gives rise to serious environmental concerns with their essential energy usage abilities [1]. All stages of fossil fuel usage have severe impact upon the environment, from recovery to storage and end use. There are alternative sources of energy being developed to replace the use of fossil fuels. Solar energy, a source of a clean environmental friendly energy and the largest available carbon-neutral energy source, can be considered as a potential solution to the environmental pollution as well as the world energy crisis. Every day, almost 400 trillion kWh energy from the sun touches surface of the earth in the form of electromagnetic radiation [2]. It does not disrupt the environment or create a threat to the eco system the way fossil fuels do.

The solar energy can be harnessed by two approaches, as passive solar technique and active solar technique. Main features of a well-deigned passive solar systems are structures, design and position, which can be optimized to use solar energy [3,4]. Active systems use mechanical and electrical equipments to utilise the solar radiation into a more usable form, such as heat or electricity [5,6]. The most well-known active solar techniques are photovoltaic panels and solar-thermal electric energy systems [7]. Though solar photovoltaics have attracted significant attention within the energy community, solar thermal energy systems recently have become prominent in the field of power generation, as such technology has proven its performance in production of clean, secure and low cost energy. These Solar thermal systems are also characterized by its simplicity in the manufacturing process, scale up potential, low technical and financial risk [8]. Unlike photovoltaic technologies, solar thermal plants have the scope to store the heat energy for some period to facilitate a successful continuous and year round supply of electricity. Solar thermal plants are usually equipped with the thermal energy storage (TES) and backup systems (BS) to provide electricity in the night hours or during cloudy days when the sun is not available [9]. Among the solar thermal technologies, concentrating Solar Power (CSP) is one of the most mature

* Corresponding author at: Nanomaterials Research Laboratory, Surface Engineering Division, CSIR-National Aerospace Laboratories, Bangalore 560017, India.
** Corresponding author at: Materials Research Centre, Indian Institute of Science, Bangalore 560012, India.
E-mail addresses: harish@nal.res.in (H.C. Barshilia), bikram@mrc.iisc.ernet (B. Basu).

http://dx.doi.org/10.1016/j.rser.2017.05.062
Received 6 January 2017; Received in revised form 6 April 2017; Accepted 15 May 2017
Available online 25 May 2017
1364-0321/

technology which has shown a great promise for the future and is currently being deployed worldwide. According to available technology road map of International Energy Agency (IEA), the CSP systems, by 2050, could provide 11.3% of global electricity with 9.6% from solar power and 1.7% from backup fuels (i.e., fossil fuels and biomass) [10].

The first commercial CSP plant was constructed by Luz International Ltd. with a capacity of 354 MW in Mojave Desert, California in the period of 1984–1991 [11]. However, efforts to duplicate similar plants suffer a setback as the reduction in fossil fuel cost dismantled the policy framework of CSP systems. A new era of CSP began in 2006 when the first central receiver tower plant, PS10, was commissioned with an overall capacity of 11 MW in Sevilla, Spain [12]. This achievement led to the approval of California Energy Commission in September 2010, for the construction of four more solar thermal power plants in California, USA, with an overall capacity around 1000 MW. The solar energy experts have estimated that CSP systems with about 118 GW could be installed by 2030 and 1504 GW by 2050 in the USA [13]. Numerous commercial projects for solar thermal plants have been taken up in Europe as well. The European Solar Thermal Electricity Association (ESTELA) estimates that the total installed capacity could reach up to 1000 GW by 2050 [14]. The government of India has also taken an initiative by launching an ambitious project, called Jawaharlal Nehru National Solar Mission (JNNSM) with a funding of USD 930 million in 2009 [15]. This project, complemented by solar policy framework, has set a goal to account for 20,000 MW solar power by 2022. The project will promote favourable conditions for solar manufacturing capability, particularly the solar thermal applications. Other countries such as China [16], Israel [17], South and north Africa [18,19], Australia [20], Algeria [21], and Italy [22] are also doing remarkable progress on current commercial development of the solar thermal plants.

The CSP technologies [23,24] can be categorised into four types depending on the way they focus the solar radiation and the technologies used to receive energy:

a. the parabolic trough collector
b. the solar tower
c. the parabolic dish concentrator
d. the linear- Fresnel reflector.

The schematic of the four types of CSP system is presented in Fig. 1. Each of these different CSP technologies have some major features along with their own advantages and drawbacks, which have been illustrated in detail elsewhere [25,26].

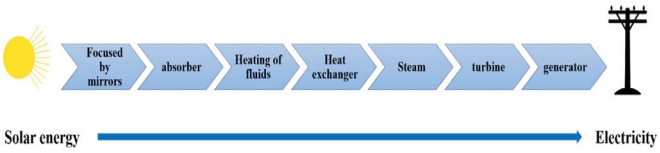

Fig. 2. Schematic of the mechanism to produce electricity from solar energy in CSP systems.

CSP plants produce electricity in the same way as other conventional power plants, but using solar radiation as energy input. In CSP systems, the solar irradiation is concentrated several times by mirrors, which have very high reflectivity to reach high energy densities. Recently, a new class of reflector materials based on Cu–Sn intermetallics with tailored substitution of aluminium or zinc with a bulk reflectance of 89% has been developed [27]. In addition, a novel δ-phase based Cu–Sn mirror through electrodeposition has been reported, the material exhibits ~ 80% of specular reflectance [28]. These mirrors would enable attaining higher temperatures in the focus of the concentrating system.

Materials that help in converting light energy harnessed from the Sun into heat are referred as absorber materials. Usually, the absorber materials are deposited onto the receiver tube, where heat transfer fluids are heated by the absorbed heat and the temperature of the fluid reaches around 400 °C. The heated fluid is driven through a series of heat exchangers to produce superheated steam. The steam is then used to operate a conventional power cycle, such as a steam or gas turbine or a stirling engine, which drives a generator (see Fig. 2).

Hence, a typical CSP system has four essential components such as concentrator, receiver or absorber, transport/storage media system (molten salt, gas, air etc.) and power conversion device. Of all components, receiver plays a vital role in determining the efficiency of the CSP systems. The nature of the absorber coating, deposited on to the receiver tube, often controls conversion of solar energy to heat. An ideal absorber should absorb as much of the incident sunlight as possible ($\alpha \geq 0.95$). This implies that the reflectance should be minimised in the entire solar spectrum. Simultaneously, the loss of the heat to the surroundings via convection or conduction, i.e. emittance ($\varepsilon \leq 0.05$), should be very low, with a thermal stability up to the operating temperature of the receiver, usually of the order of 400 °C. Thus, there are conflicting requirements of strong absorption in the solar spectrum, with minimum emission in the far infrared range (Fig. 3).

The design of the absorber surfaces initially attracted attention

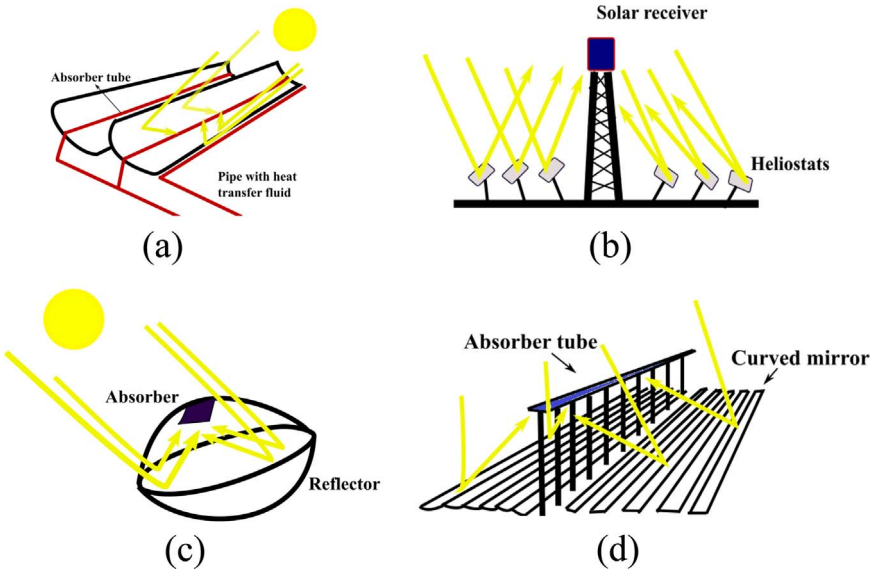

Fig. 1. Schematic of four CSP systems a) parabolic trough collector b) solar tower c) parabolic dish concentrator and d) linear Fresnel reflector [23,24].

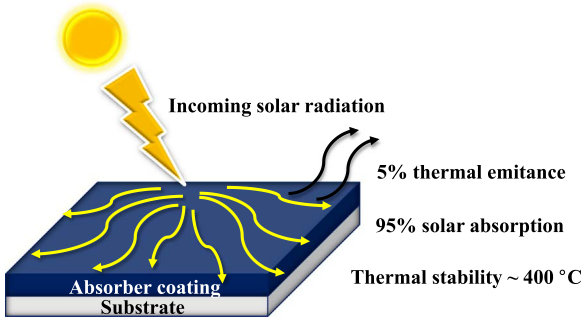

Fig. 3. Schematic of an ideal solar selective absorber.

while Kemp patented lamp black as an absorber material in a solar water heating device in 1891 [29]. This is followed by a number of invention disclosures dealing with solar water heating systems that were filed in USA during the first half of the 20th century [30–32]. The black painted tubes were used as collectors in these systems. However, the development of the modern solar absorber coating can be traced to the invention of Tabor in 1955 when black nickel, NiS–ZnS composite, black chrome and chemically converted black copper oxide were electrodeposited on an infrared reflective aluminium substrate [33]. Since then, several deposition procedures like physical vapour deposition [34], chemical vapour deposition [35], electro deposition [36], sol-gel [37], paint-coating [38] etc., have been pursued to meet the criteria of solar selective coating. A variety of coating structures such as intrinsic absorbers, semiconductor absorbers, multilayer absorbers, metal-dielectric composite absorbers, texture surfaces and dielectric-metal-dielectric (DMD) absorbers have been extensively studied to increase the efficiency of photo-thermal conversion systems.

In a review published in 1983, Bogaerts and Lampert [39] reported commercially or potentially available selective and non-selective absorber surfaces for solar heat collectors. In the same year, Niklasson and Granqvist [40] summarized the development in the solar selective coatings that were reported during 1955–1981. In 2002, an exhaustive review emphasising the application of solar selective coating in different temperature was published by Kenedy [41], while Granqvist [42] in 2003 reported potential materials that could be utilised in photo-thermal as well as photo-electric applications. Several other reviews are available on the subject including the work of Agnihotri and Gupta [43], Granqvist and Wittwer [44], Goswami et al. [45], Amri et al. [46], Atkinson et al. [47] and Jeeva et al.[48]. In 2012, Selvakumar and Barshilia [49] extensively reviewed a wide variety of physical vapour deposited (PVD) solar selective absorber coatings, their functionality, reliability and performance at elevated temperatures. They also summarized commercially available PVD coatings for flat-plate/evacuated tube collectors and solar thermal power generation applications. However, there is a need for a review focused on the dielectric-metal-dielectric (DMD) –based absorber coatings with the underlying physics of surface plasmon polaritons (SPPs) because of their increasing importance in future solar conversion technologies. In the current review, we present theoretical background of SPPs in designing metal-dielectric interface and present an overview of the understanding of imparting solar selectivity. We demonstrate the contextual analyses of DMD –based solar absorber coating, their performance and the future directions of research that can be undertaken in harnessing the solar energy in the collector of the photo-thermal conversion systems.

This article is set out as follows: The solar absorptance and the thermal emittance are the most important properties that can significantly influence the solar selectivity of absorber coating. Hence, to provide a contextual backdrop for this review, we have discussed the correlation of solar absorptance and thermal emittance with the solar selective properties of the absorber coating in Section 2. Different types of solar selective absorber coatings, their examples and possible theoretical description on individual coatings have been presented in Section 3. In the same section, we have also discussed different models, which can explain the metallic and dielectric properties of the materials in a DMD stack. Section 4 is devoted in describing SPP, the dependence of relative permittivity, refractive index, thickness etc., on the dispersion relation of SPP, the effect of metal-dielectric (MD) and dielectric-metal-dielectric structure (DMD) on SPP behaviour, the impact of DMD structure in the absorption of solar energy. We then give a detail overview on varieties of DMD –based solar selective absorber coatings, explored by several groups and their selective properties, thermal stability and applicability to enhance the efficiency of CSP systems in Section 5. Section 6 demonstrates an idea to develop textured DMD –based absorber coating which may possess significantly improved selectivity than a flat DMD coating. Finally, we have highlighted the critical parameters which govern the environmental stability, cost-performance factor, practical implantation of the DMD coatings in CSP systems to boost the demand of safe and affordable energy.

2. Physics of solar selectivity

In 1865, Maxwell first proposed the classical theory of electromagnetism and predicted light as electromagnetic radiation [50]. The electromagnetic spectrum can be further classified into different types depending on the range of wavelength varying from cosmic and gamma rays (wavelength ~ 10^{-8} μm) to long radio waves (wavelength ~ 10^{10} μm). The electromagnetic radiation, emitted by sun is known as solar spectrum, and it falls in the wavelength range of λ = 0.3 ~ 2.5 μm. The radiation emitted from bodies at temperature of 200 °C and above spreads in the infrared region of the spectrum, which extends from λ = 2.5 ~ 50 μm. Specifically, two parts of electromagnetic spectrum, such as solar radiation and thermal radiation, are important for solar selective absorber coating.

2.1. Solar absorptance

When light, an electromagnetic (EM) wave, incidents on a material, it interacts with the atoms, ions and/or electrons in the material, and the corresponding effects depend on the frequency of the light and the atomic structure of the material. Light - matter interaction causes three common physical phenomena such as absorption, reflection and transmission, as shown in Fig. 4. The disappearance of EM wave inside the medium is known as absorption. Absorption occurs when the energy of an incident photon is equal to the band gap of the material.

The term absorptance, is defined as the ratio of the radiation absorbed by the body or surface to the incident solar radiation and can be expressed,

$$\alpha_\lambda(\lambda) = \frac{G_{\lambda,abs}(\lambda)}{G_\lambda(\lambda)}, \quad (1)$$

where $G_{\lambda,abs}(\lambda)$ and $G_\lambda(\lambda)$ are the absorbed and incident radiations, respectively.

Conservation of energy demands that the sum of the transmission, reflection, and absorption of the incident flux is equal to unity. Therefore, the total radiation can be characterized by the following equation

$$\alpha_\lambda + \rho_\lambda + \tau_\lambda = 1, \quad (2)$$

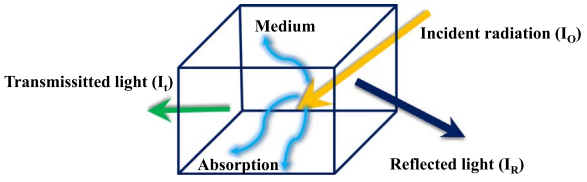

Fig. 4. Interaction of electromagnetic radiation with matter.

where α_λ, ρ_λ and τ_λ are the absorptance, reflectance and transmittance at a given wavelength. For materials that does not allow the penetration of the incident radiation through it, i.e. while the transmittance is equal to zero ($\tau_\lambda = 0$), the Eq. (2) get reduced to

$$\alpha_\lambda + \rho_\lambda = 1 \tag{3}$$

$$\alpha_\lambda = 1 - \rho_\lambda \tag{4}$$

Using Eqs. (1) and (4), the absorptance can be expressed in terms of reflectance by the following equation

$$\alpha(\theta) = \frac{\int_{\lambda_1}^{\lambda_2} [1-\rho_\lambda] G(\lambda) d\lambda}{\int_{\lambda_1}^{\lambda_2} G(\lambda) d\lambda}, \tag{5}$$

where λ is the wavelength, θ is the incident angle of light, λ_1 and λ_2 are minimum and maximum solar wavelengths, respectively. The absorptance of a solar selective coating is usually determined by the reflectance spectra of the coating, obtained using standard UV–Vis–NIR spectrophotometer. The reflectance spectra is generally measured in the solar wavelength range of 0.3–2.5 μm and at near normal angle of incidence ($\theta = 0°$).

2.2. Thermal emittance

All objects emit electromagnetic radiation. However, before defining the term "thermal emittance", it will be useful to introduce the definition and physical properties of a perfect black body [51]. An ideal blackbody is a hypothetical object that absorbs all radiation incident on it. The expression of the radiant energy distribution from a perfect blackbody was proposed by Max Planck in 1901. Plank's law can be represented as

$$E_{b\lambda}(\lambda, T) = \frac{8\pi hc}{\lambda^5 \exp\left(\frac{hc}{\lambda k_B T} - 1\right)}, \tag{6}$$

where c, h and k_B are the speed of light (m/s), Planck's constant (J-s) and Boltzman's constant (J-K^{-1}), respectively.

The variation of radiant power density of the blackbody at 100, 200 and 300 °C is shown in Fig. 5. Some of the observations can be pointed out as,

a. the emitted radiation is a continuous function of wavelength. At a given temperature, it increases with wavelength, reaches a peak and then decreases with increasing wavelength.
b. at any wavelength, the radiation increases with an increase in temperature.
c. when temperature increases from 100 to 300 °C, a shift in the maxima of the curve is observed towards shorter wavelength.
d. the solar spectrum, presented in the same curve is considered to be a black body at approximately 5800 K.

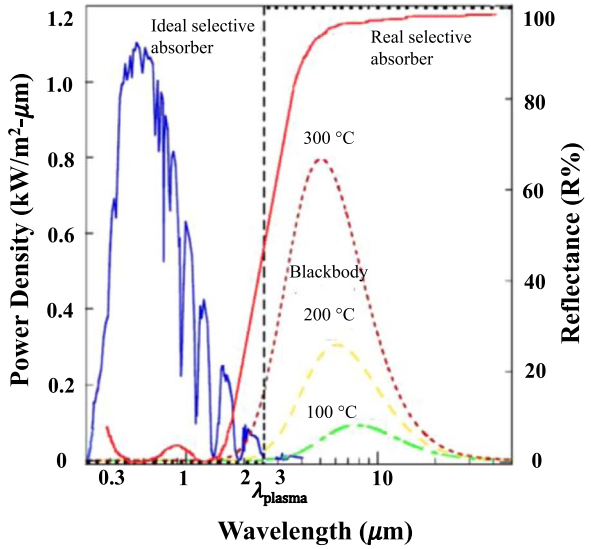

Fig. 5. The solar spectrum (blue); the blackbody radiation at 100, 200 and 300 °C (green, yellow, maroon, respectively); The reflectance spectrum of an ideal (black) and real (red) solar selective absorbers [46].

The important fact is that the total radiation from the black body can be calculated by integrating the blackbody spectrum over the entire wavelength range. This is known as Stefan-Boltzmann law [52], given as

$$E_b(T) = \int_0^\infty E_{b\lambda}(\lambda, T) d\lambda = \sigma T^4, \tag{7}$$

where σ is the Stefan-Boltzmann constant.

The above expression suggests that the total emissive power of a blackbody is proportional to the fourth power of its temperature. Therefore, emittance or thermal radiation from a black body increases drastically with a small increase in the temperature.

The emittance (ε) of a surface is represented by the ratio of radiation emitted by the object at a given temperature (E_λ) to the radiation emitted by a perfect blackbody ($E_{b\lambda}$) at the same temperature. It is a dimensionless number that ranges from 0 to 1 i.e. $0 \le \varepsilon \le 1$. It is a measure of how strongly a material radiates at a given wavelength and how closely a material approximates an ideal blackbody for which ε = 1. The emittance of a physical body depends on its temperature, chemical composition, surface roughness, intrinsic geometrical structure, the wavelength to which the emitted radiation corresponds and the angle at which the radiation is emitted. The total hemispherical emittance can be expressed as,

$$\varepsilon_\lambda(\lambda, T) = \frac{E_\lambda(\lambda, T)}{E_{b\lambda}(\lambda, T)} \tag{8}$$

Kirchhoff's law, on the other hand, states that the total hemispherical emittance (λ) of a surface at temperature T is equal to it's total hemispherical absorptance α(λ) from a blackbody at the same temperature. Therefore, the emissivity of a coating can be determined by the absorptance of a coating in the infrared wavelength range. Using Eq. (4), the emittance (ε) can be obtained by the following equation

$$\varepsilon_\lambda(\lambda) = \alpha_\lambda(\lambda) = 1 - \rho_\lambda(\lambda) \tag{9}$$

Combining Eqs. (8) and (9), the emittance of a coating at a temperature, T can be calculated in terms of the reflectance,

$$\varepsilon(T) = \frac{\int_{\lambda_1}^{\lambda_2} [1-\rho_\lambda(\lambda)] E_{b\lambda}(\lambda) d\lambda}{\int_{\lambda_1}^{\lambda_2} E_{b\lambda}(\lambda) d\lambda}, \tag{10}$$

where $E_b(\lambda)$ is the black body radiation spectrum. The spectral range of thermal radiation emitted from a surface having a temperature of about 300 °C is found from 2.5 to 25 μm are used as λ_1 and λ_2, respectively. The emittance of the absorber coating can be obtained using the diffuse reflectance spectra in the wavenumber range of 400–4000 cm^{-1} (2.5–25 μm) using FTIR spectrophotometer.

For CSP applications, the absorber materials should have high absorptance (α) > 0.95 in the solar spectrum (0.3–2.5 μm) and low thermal emittance (ε) < 0.05 in the thermal radiation region i.e. infrared region (2.5–25 μm). The ratio of solar absorptance to thermal emittance is also known as spectral solar selectivity (α/ε). The spectral performance of an ideal selective solar absorber should be a step function, illustrated in Fig. 5. Fig. 5 clearly indicates a step at 2.5 μm below which (solar spectrum) reflectance ρ=0 and above (infrared region) ρ=1. The particular wavelength, where the step starts is known as plasma wavelength, λ_{plasma}. For real selective absorber, a slight difference in the pattern of the step, plotted by red colour can be observed.

3. Performance evaluation of absorber coatings

While independent measurements of absorptance, emittance and selectivity are routinely conducted for any new bulk material/coating, a few attempts are made to define some of the performance qualifying parameters to integrate the basic properties of relevance. This section highlights a few such functions or parameters.

3.1. Merit function and absorber efficiency

Sergeant et al. [53] proposed the merit function, {F(T)}usy of an absorber coating in terms of absorptance (α), emittance (ε) and the operating temperature (T) by the following relation

$$F(T) = [1 - \varepsilon T] \tag{11}$$

Therefore, higher the α and lower the ε, better is the F(T) value. Also, the spectral selectivity of an absorber coating increases with an increase in merit function. The cut off wavelength, λ_{plasma} can also be determined by the merit function. Solar to thermal conversion efficiency for an ideal selective absorber, $\eta_{sol\text{-}the}$ at a particular temperature (T) has been defined by Cindrella [54] and Ho et al. [55],

$$\eta_{sol-the} = \alpha - \frac{\varepsilon(T)\sigma T^4}{CI_s} \tag{12}$$

where C is the concentration ratio which is usually on the order of 10–1000, I is the solar flux density (W/m^2) and σ is Stefan-Boltzmann constant [56]. The cut off wavelength can also be calculated as a function of operating temperature. It has been observed that a combination of higher concentartions and lower operating temperatures lead to longer wavelength cut offs, while the opposite conditions provide a shorter wavelength cutoffs. Therefore, for a specific solar selective absorber, it is necessary to maximize the overall solar-thermal efficiency by considering a specific structure, material, working temperature and the concentration factor [57].

3.2. Levilized cost of coating (LCOC)

Ho et al. have found out an innovative way to evaluate annual performance, cost, and reliability/durability of selective coating by introducing a new parameter called Levilized Cost of Coating (LCOC) [58]. This can be defined as the ratio of total annualized coating cost to the annual thermal energy absorbed (MWh_{th}) by the receiver,

$$LCOC = \frac{C_{annual}}{E_{thermal}} \tag{13}$$

where,

C_{annual} = total annualized coating cost

= initial coating cost/life of plant + recoating cost/recoating interval + cost of additional (or fewer) heliostats to yield a baseline thermal energy production

$E_{thermal}$ = average annual energy absorbed

= annual thermal energy absorbed (new) − annualized lost energy absorbed due to degradation − annualized lost energy absorbed due to down time for re-coating

Along with the solar-thermal conversion efficiency, $\eta_{sol\text{-}the}$ and other parameters like the degradation rate, material cost, reapplication cost etc. have a huge impact on LCOC.

4. Solar selective absorbers : Generic classifications

Over the last few decades, preparation of absorber coating has become a popular topic of research. A number of materials have been investigated as absorber coatings till date. The selection of the material, structures and fabrication procedures etc., determine the selective performance of the absorber coatings. However, the main challenge of the absorber lies on the performance of the coating at high temperature. Therefore, along with the solar selectivity few more desired properties of the absorber coatings include,

a) high temperature stability (~ 400 °C)
b) corrosion and humidity resistance
c) ability to prevent oxidation
d) high structural and chemical stability
e) hardness and scratch resistance etc.

Among all these properties, the high temperature stability is a prime criteria for a potential solar selective absorber coating.

A number of different design principles and physical mechanisms can be used to develop spectrally selective solar absorbing surfaces. Depending on the design principle, the solar selective surfaces can be categorized in a number of different types including intrinsic absorber, semiconductor coatings, multilayer coatings, metal-dielectric composite coatings, textured surfaces and most importantly DMD -based coatings. The schematic diagrams of these absorber coatings have been presented in Fig. 6. In the following, some of the coating types and their operating principles are briefly described.

4.1. Intrinsic absorbers

As the name suggests, intrinsic absorbers inherit selectivity as a property. The examples include V_2O_5 [59], LaB_6 [60], Fe_3O_4 [61], Al_2O_3 [62], few ultra-high temperature ceramics (UHTCs), for example, ZrB_2 [63], ZrC, TaC, HfC [64], SiC, ZrB_2, HfB_2 [65] etc. These materials have attracted attention as potentially suitable candidates for solar selective application. The primary component of most of these materials are from transition metal or lanthanide group. They usually have many available orbitals at energy levels compatible with the energy of visible light. Recently, Ankit et al. [66] explored the intrinsic selectivity of W by laser sintering of micro and nano particles of W on stainless steel. The coating showed excellent performance even after heat treatment at 650 °C in air for 36 h. Few researchers have reported the intrinsic selective property of single-walled and multi-walled carbon nanotubes [67,68]. Some of the paint coatings or electrodeposited coatings made of spinel pigments, such as $CuAl_2O_4$ [69], $CoCuMnO_x$ [70], $Cu_{1.5}Mn_{1.5}O_4$ [71], Mn-Fe spinel PK 3060 [72], $CuCr_xMn_{2-x}O_4$ [73], $CuCr_2O_4$ [74], $NiCo_2O_4$, $FeCo_2O_4$, $CoFe_2O_4$, $CuCo_2O_4$, $(NiFe)Co_2O_5$, $Co_{1.5}Fe_{1.5}O_4$ [75] also show selective property. They exhibit an absorptance of 0.80 and emittance of 0.20 up to 100 °C [76]. A drawback of using most of the intrinsic absorbers is that the crossover from low to high wavelengths, i.e. the step in the reflectance spectra occurs at too short wavelengths or the slope at the transition wavelength is not so steep. In addition, the low thermal conductivity of these materials (except UHTCs) is not suitable for high temperature applications. Moreover, a thick layer of the intrinsic material is needed to absorb maximum solar energy, while the increase of the thickness causes an increase in emittance. These problems can be overcome by introducing a structural or compositional change in the lattice of these materials. Therefore, the properties of the intrinsic materials should be tailored to satisfy the specific needs by doping a suitable element inside the material or preparing composites with some other materials. Doping enhances the selectivity by two ways, firstly the donor atoms give rise to electron plasma, and secondly, these donors act as a scattering centre, which enhances the optical path of solar radiation and leads to maximum absorptance. For example, the doping of W in VO_2 matrix ($V_{1-x}W_xO_2$) makes it suitable as solar thermal absorber [77]. A femtosecond laser treated composite coating of 70 vol% HfC - 30 vol% $MoSi_2$ exceled itself as a promising selective absorber [78]. Fang et al. [79] demonstrated that Ti_3SiC_2 and $Zr_3[Al(Si)_4]C_6$ have lower emissivity and better thermal stability than TiC and ZrC ceramics. Xu et al. [80] presented cordierite ($2MgO.2Al_2O_3.5SiO_2$)/SiC composite as potential solar selective absorber material due to excellent solar selectivity and thermal shock resistance.

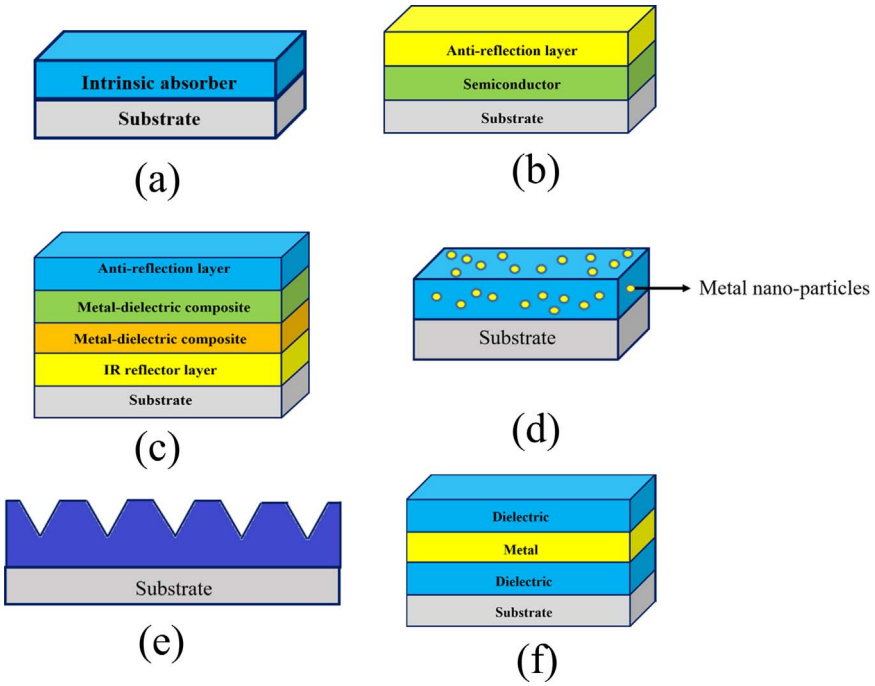

Fig. 6. Different types of solar selective absorber coatings; (a) Intrinsic absorber, (b) Semiconductor absorber, (c) Multilayer absorber, (d) Cermet absorber (e) Textured surface (f) Dielectric – metal – dielectric –based absorber [42].

4.2. Semiconductor absorbers

The particular interest on semiconductor absorber has been focused on the semiconductor with the band gap (E_g) in the range of 0.5 eV (2.5 μm) to 1.26 eV (1.0 μm) such that the plasma wavelength λ_{plasma} lies in the desired position. Thus, some of the semiconductors Si (1.1 eV), Ge (0.7 eV), PbS (0.4 eV) have good potential as absorber materials in solar thermal applications [81]. A novel absorber $Si_{0.8}Ge_{0.2}$ with a band gap of 1.04 eV has been reported by Moon et al. [82] and such absorber exhibited a solar absorptance of 0.90–0.95, while maintaining a relatively low emittance of less than 0.3. Yang et al. [83] proposed a Ge check board structure on Ta substrate using finite-difference time domain (FDTD) method, which shows very high absorptance below 1.2 μm and less absorptance beyond that. Xiao et al. [84] have taken advantages of the semiconductor nature of copper oxide (CuO, Cu_2O). The band gap of the p-type semiconductor, CuO and Cu_2O are 1.4 and 2 eV, respectively. They have developed the copper oxide coating by one-step chemical conversion method and the highest photo-thermal efficiency was achieved with an absorptance of 0.94 and an emittance of 0.08. The underlying metallic layer helps to reflect the infrared wavelength and reduces the emissivity.

The disadvantage of the semiconductor coatings is their high refractive index, which causes large reflectance loss, and as a result, the coating can absorb less amount of solar energy. The performance of such coatings can be improved by depositing an antireflection coating on top of the semiconductor. A single layer AR coating of MgF_2, SiO_2, Al_2O_3 [85], TiO_2, [86] Si_3N_4 etc., can be deposited on the semiconductor to reduce the loss of absorbed energy from the coating surface. Seraphin et al. [87] fabricated a semiconductor-based multilayer coating of $SS/Cr_2O_3/Ag/Cr_2O_3/Si/Si_3N_4/SiO_2$ by chemical vapour deposition, where Si served the role of main absorber layer and Si_3N_4 and SiO_2 layer acted as anti-reflection layer. The coating exhibited an absorptance of 0.85 and emittance of 0.07 with a high thermal stability up to 500 °C.

4.3. Multilayer absorbers

The most elementary systems, like intrinsic or semiconductor absorber coatings are not suitable for high temperature applications. Therefore, in recent years, the coatings with the multilayers structures have been considered as reliable in the high temperature applications. A multilayer coating consists of several alternative layers of dielectric and semi-transparent metallic layers. The dielectrics usually absorb well in the visible wavelength range and the metals reflect the infrared. Anti-reflection coatings are usually put on top to improve transmission to the absorbing layers. High absorptance up to 0.95 and low emittance of 0.05 can be achieved by the multilayer stack even under elevated temperature conditions.

In a multilayer coating, superposition of multiple light waves introduce interference, which depends on the relative phase of each light wave. Destructive interference prevents the reflectance of the light and enhances absorptance in thin films. Destructive interference occurs when two interfering waves with 180° phase difference superpose each other. However, this phase difference for destructive interference correlates to a λ/2 shift of the sinusoid wave that is best achieved by adjusting the optical thickness of the layer, a function of layer thickness. The above discussion emphasises that the thickness of individual layer in a multilayer coatings needs to be approximately tailored to obtain desire combination of solar selective properties.

In recent years, the transition metal of group IVA, VA, and VIA and their nitride/oxynitride/oxide based coatings have attracted significant attention as stable high temperature absorber coating. The metal volume fraction and the refractive index of each layer of these coatings usually increase from surface to substrate to enhance absorptance. The metal volume fraction can be varied by the deposition time, target power and gas flow rate. A large number of multilayer coatings such as $TiAlN/CrAlON/Si_3N_4$ [88], AlCrSiN/AlCrSiON/AlCrO [89], TiAlSiN/TiAlSiON/SiO_2 [90], HfMoN(H)/HfMoN(L)/HfON/Al_2O_3 [91], Mo/AlCrON(HMVF)/AlCrNO(LMVF)/$AlCrO_x$ [92], $Al_2O_3/Cu/Al_2O_3$/AlCuFe [93], $Ti_xAl_{1-x}/(TiN\text{-}AlN)_H/(TiN\text{-}AlN)_L/AlN$ [94], $Ti_{0.5}Al_{0.5}N/Ti_{0.25}Al_{0.75}N/AlN$ [95], TiAlCrN/TiAlN/AlSiN [96] have been devel-

oped by several groups. We have recently developed a W/WAlN/WAlON/Al_2O_3 multilayer absorber coating that had a very high absorptance of 0.958 and low emittance of 0.08. The coating showed very high stability at 350 °C in air for 550 h [97–99]. TINOX [100] (sputtered titanium nitride film) developed by ALMECO group [101] is commercially available and notable among these multilayer absorber coatings that exhibit an absorptance of 0.95 and emittance of 0.04.

The main disadvantage of multilayer structure are the high fabrication cost. These coatings can be manufactured by the simple, advantageous and up-scalable wet chemistry method to reduce the production cost. In order to prove feasibility of fabricating multi-layer coating by wet chemistry method, Bayon et al. [102] deposited CuMnSiOx/CuMnOx/SiO_2 coating on Al substrate by dip-coating and achieved the absorptance of 0.95 that can compete with the commercially available sputter coated absorber. The coating also qualified the long-term thermal stability test. Recently Joly et al. [103] reported a Cu-Co-Mn-Si-O -based graded index coating by sol-gel method that showed high selectivity of 0.95/0.12 with a high thermal stability and corrosion resistance. Therefore, it can be commented that fabrication of multilayer coating by wet chemistry route can provide a direction towards the future commercialization of the selective coating.

4.4. Cermets or metal-dielectric composite absorbers

Cermets, i.e. metal-dielectric composites, consist of nanoscale metal particles in a dielectric or ceramic matrix. The multilayer coatings and cermets have similarity as dielectric material is used in both the structure for the solar absorption, while metal serves as infrared reflector. The metal particles in absorber coatings play an important role by acting as a modifier for the optical response of the ceramic phase. The solar radiation is scattered by the boundaries between the metallic and dielectric phase. As a result, the optical path length of the radiation increases, which leads to an increase in the absorption by a factor of $4n_d^2$, where n_d is the refractive index of the dielectric medium [104]. The light trapping in the cermet also occurs due to quantum confinement effect and is known as surface plasmon resonance phenomenon (SPR) [105]. SPR is the collective oscillations of the conduction electrons of metal nanoparticles in the dielectric matrix that influences the optical absorption in the solar spectrum.

Critical parameters for an efficient cermet coating are the dielectric constant of the metal nanoparticles and the dielectric matrix [106]. Dielectric function of the composite can be calculated theoretically by the following equation obtained from Maxwell-Garnett (MG) [107] and Bruggeman theory (BR) [108], considering the identical spherical grain with the size much less than the wavelength of light:

$$\varepsilon^{MG} = \varepsilon_B \frac{\varepsilon_A + 2\varepsilon_B + 2f_A(\varepsilon_A - \varepsilon_B)}{\varepsilon_A + 2\varepsilon_B - f_A(\varepsilon_A - \varepsilon_B)} \text{and} \quad (14)$$

$$f_A \frac{\varepsilon_A - \varepsilon^{BR}}{\varepsilon_A + 2\varepsilon^{BR}} + (1 - f_A)\frac{\varepsilon_B - \varepsilon^{BR}}{\varepsilon_B + 2\varepsilon^{BR}} = 0, \quad (15)$$

where ε^{MG} and ε^{BR} represent the average dielectric functions of the composite in MG and BR approximations, ε_A and ε_B indicate the dielectric function of metal (A) and ceramic (B). The metal filling factor f_A is the volume fraction occupied by metal. If f_A is less than zero, MG theory can be used to calculate the dielectric constant of composite cermet. BR theory is used otherwise. In order to get accurate value of the dielectric constant, ellipsometry measurement can be performed. Generally Mo, Pt, W, Cr, etc., are used as metallic components in SiO_2, Al_2O_3, Cr_2O_3, TiO_2, AlN matrix [109–112].

In order to improve the optical performance and thermal stability, researchers have developed cermets that are composed of four layers consisting of (i) an infrared reflective metallic layer (IR-mirror), (ii) a high metal volume fraction (HMVF) cermet, (iii) a low metal volume fraction (LMVF) cermet layer, and (iv) an anti-reflective (AR) layer [113]. Such kind of cermets, like W-Al_2O_3 [114], AlNi-Al_2O_3 [115], Ag-Al_2O_3 [116], Pt-Al_2O_3 [117] Mo-Al_2O_3 [118], Mo-SiO_2 [119,120], Ni-NiO [121], and W-Ni-YSZ [122] have been reported for solar selective absorber coatings. Among the successful selective coatings, a few are commercially available for high temperature applications. For example, Mo-Al_2O_3 and W-Al_2O_3 have been commercialized by Siemens (Germany) due to their thermal stability in the range of 350–500 °C [123,124]. Mo-SiO_2 and W-Al_2O_3 have been commercially used by Angelantoni ENEA (Italy) and Turbosun (China) commercializes AlN-based ceramics [125,126].

However, most of the reported cermet coatings have been fabricated by sputtering, evaporation or chemical vapour deposition. The essential requirement of an optically efficient solar selective coating is cost-effectiveness. Therefore, the cermets coating deposited by electrodeposition or sol gel method have been extensively investigated. Wang et al. [127] have proposed preparing Ni-nanochain-Al_2O_3 coating using solution chemical process. The coating had a solar absorptance > 0.90 and a low thermal emittance < 0.10. In a separate study, Katumba et al. [128,129] have utilised the embedded amorphous and shapeless carbon in three different metal oxides (C/SiO_2, C/ZnO, and C/NiO) by sol-gel method. They found that C/NiO cermet exhibits superior selective properties with the solar absorptance of 0.93. Roro et al. [130] believed that the selective property can also be achieved by replacing amorphous carbon by multi-walled carbon nanotubes. The best solar absorptance and the thermal emittance of MWCNTS/NiO obtained were 0.84 and 0.2. The electrodeposited Co-Al_2O_3, prepared by Cuevas et al. [131] demonstrated a high absorptance of 0.92 and emittance of 0.16. Co-Al_2O_3 structure has been engineered in such a way so that Al_2O_3 pores have been filled by Co nano particles. The review article of Cao et al. [132] provides ample evidence of the cermet based absorber coating in detail.

4.5. Absorbers with textured surfaces

Most of the solar selective coatings reported in literature are multilayer coatings or cermet structures. Though the optical performance of these coating is superior, these designs fail at high temperatures (> 1000 K) due to oxidation, substrate diffusion, intra and interlayer reactions of the constituent element and thermo mechanical stresses between the layers and interfaces. To overcome the aforementioned shortcomings while keeping the selective property unaffected, surface texturing appears to be a technologically emerging approach [133]. Textured surface with porous, granular, dendrite or needle-like microstructures is capable of producing very high absorptance, capturing solar energy by multiple reflections, while low emittance can be achieved as the surface seems to be smooth for longer wavelengths [134].

Chen et al. [135] developed tapered aluminium doped zinc oxide nanorod arrays using electrodeposition which exhibited absorptance of 0.95 in the solar spectrum. The 1D CuO nanostructures like nanofibers and nanoneedles, fabricated using chemical oxidation of Cu exhibited a selectivity of 0.95/0.07 [136]. Sergeant et al. [137] proposed a design of sub-wavelength V-groove gratings coated with aperiodic metal-dielectric stacks, which could have absorptance > 0.94 and emittance < 0.06 at 720 K. Photonic crystals [138] and metamaterials [134] have also been designed considering the challenge of stability in the high temperature and long span of operation. Wang et al. [139] simulated optical properties of a two-dimensional (2D) Mo photonic crystal (PhC) surface that exhibited a high absorptance of 0.919 and low emittance of 0.149 at 1000 °C. Rigorous Coupled-Wave Analysis (RCWA) method was used to optimize the spectral property of the system by varying the diameter, height and periodicity of the Mo column cells. In another study, a selective metamaterial absorber made of a 2D titanium grating deposited on an MgF_2 spacer and an opaque tungsten film showed an absorptance and emittance of 0.9 and 0.2, respectively, with a thermal stability up to 350 °C [140].

4.6. Dielectric-metal-dielectric (DMD) absorbers

The ray-optics theory of light trapping using multiple reflections (in case of multilayer film or the texturing of the surfaces) is becoming traditional. Moreover, the long wavelength leaves these coatings due to specular reflection from the rear surface. In order to reduce the large loss of escaping long wavelength light, the optical path length of weakly absorbed light has to be enhanced. The DMD structure, which is another type of selective coating, can be employed to improve the absorption by the use of Surface Plasmon Polaritons (SPPs) [141,142]. SPPs provide a tuneable high scattering cross section at larger angles and increase the optical path length. It is also worth developing light-trapping layers like DMD absorber, which is based on wave-optics in a scalable fashion. The challenge of developing such layers is to identify tuneable compositions that can bridge the gap between the optical properties of metals and dielectrics and increase the solar absorption without increasing any thermal heat loss.

A key advantage of such a coating is the small amount of material required to fabricate the structure, which reduces consumable costs. As the high temperature stability is concerned, stable nanocrystalline or amorphous dielectric materials (Cr_2O_3, MgO, Al_2O_3) are highly desirable. Based on the melting point and resistance against oxidation in high temperature, metals like Cr, Mo, Al, Pt, etc., are the ideal candidates for DMD absorber layers.

Most of the studies on DMD -based absorber structures have shed light on some parameters like refractive index (n), extinction coefficient (k), and thickness of individual layer. The amplitude ratio of parallel and perpendicular components of the reflected wave (Ψ) from the coating and their relative phase change (Δ) can be obtained from the spectroscopic phase modulated ellipsometry over a particular wavelength range (300–1200 nm). Some predictive models (Tauc-Lorentz interband transition model [143], Adachi's model [144], user-defined expressions for optical constants, imported dielectric functions, classical Drude model [145] etc.) can be fitted with the experimental elliposmetry data to quantify the optical constants (n and k) of metal and dielectric which influence the overall performance of the selective coatings. Using these models, researchers predict and investigate the optimum combination of the metal and dielectrics to develop highly efficient DMD -based absorbers.

In order to derive the dispersion relation for complex dielectric function of semiconductor material, Ninomiya and Adachi [146,147] correlated the energy band structure and imaginary part of the complex dielectric function. The dispersion relation can be expressed as

$$\varepsilon(E) = \frac{4e^2\hbar^2}{\pi\mu^2E^2}\int dk|P_{cv}^2|\delta[E_c(k)-E_v(k)-E], \tag{16}$$

where μ is the combined density of state mass, Dirac δ function represents the joint spectral density of state between the valence, the valance band E_v(k) and the conduction band E_c(k) states differing by the incident energy $E = \hbar\omega$, P_{cv}**(k)** is the momentum matrix element between valance and conduction band states, which has been evaluated by the integration over the first Brillouin zone.

The analytical expression for the dielectric constant can also be obtained from TL dispersion model [148], which has been extensively used to describe the dispersion of optical constants in case of amorphous and nanocrystalline dielectric materials. The imaginary part of the dielectric function ($\varepsilon_2 = 2nk$) of the material can be expressed as,

$$\varepsilon_{2TL}(E) = \frac{A_{TL}E_OC_L(E-E_g)^2}{(E^2-E_O^2)+C_L^2E^2}, \tag{17}$$

where E_O is the peak transition energy, while A_L and C_L determine the strength and broadening of the transition, respectively.

The expression for real part of dielectric constant ($\varepsilon_1 = n^2-k^2$) can be obtained by Kramers–Kronig analysis as:

$$\begin{aligned}\varepsilon_{1TL}(E) &= \varepsilon_{1TL}(\infty)+\frac{1}{2}\frac{A_{TL}}{\pi}\frac{C_L}{\xi^4}\frac{\alpha_{ln}}{\alpha E_O}\ln\left[\frac{E_O^2+E_g^2+\alpha E_g}{E_O^2+E_g^2-\alpha E_g}\right]\\ &- \frac{A_{TL}}{\pi\xi^4}\frac{a_a tan}{E_O}\left[\pi - a\tan\left(\frac{2E_g+\alpha}{C_L}\right)+a\tan\left(\frac{-2E_g+\alpha}{C_L}\right)\right]\\ &+ \frac{2A_{TL}E_O}{\pi\xi^4 a}\left\{E_g(E^2-\gamma_{TL}^2)\left[\pi+2\text{atan}\left(\frac{2\gamma_{TL}^2-E_g^2}{\alpha C_L}\right)\right]\right\}\\ &- \frac{A_{TL}E_OC_L}{\pi\xi^4}\frac{E^2+E_g^2}{E}\ln\left(\frac{|E-E_g|}{E-E_g}\right)\\ &+ \frac{2A_{TL}E_OC_L}{\pi\xi^4}E_g ln\left[\frac{|E-E_g|(E+E_g)}{\sqrt{(E_O^2-E_g^2)^2+E_g^2C_L^2}}\right]\end{aligned} \tag{18}$$

The details of this expression can be found elsewhere [149]. The n and k of metallic layer can be modelled by Cauchy's dispersion formula [150], represented by the following equations:

$$n(\lambda) = A+\frac{B}{\lambda^2}+\frac{C}{\lambda^4}\text{and} \tag{19}$$

$$k(\lambda) = D+\frac{E}{\lambda^2}+\frac{F}{\lambda^4}, \tag{20}$$

where A-F are the parameters of dispersion relation and λ is the wavelength of incident light. The dispersion relation of metal can also be fitted by Drude –type dispersion relation [151], represented by

$$\varepsilon_M = \varepsilon_\infty+\frac{\omega_p^2}{-\omega^2+i\Gamma_D\omega}, \tag{21}$$

where ε_M is the complex dielectric constant of metal, ε_∞ is the high-frequency component of the dielectric constant, ω_p is the plasma frequency and Γ_D is the damping factor.

In order to investigate optical properties of metal and dielectric thin films, the measured ellipsometric spectra needs to be fitted with theoretically generated ellipsometric spectra by varying thickness and parameters of dispersion relation of aforementioned practically useful predictive models. Full analysis of the optical constants using the comprehensive models have been performed for a number of DMD systems, such as $Cr_xO_y/Cr/Cr_2O_3$ [152], $Al_xO_y/Al/Al_xO_y$ [149], $HfO_x/Mo/HfO_2$ [153] etc. The variation of the optical properties (n and k) of the individual layer with respect to wavelength satisfy the general characteristics of metals and dielectrics.

5. Characteristics of surface plasmon polaritons in dielectric–metal–dielectric structure

In a pioneering work, Ritchie [154] first introduced the self-sustained coherent electron oscillations at the metal surface in 1957. After two years, Powell and Swan [155] proved the existence of these collective excitations by some electron energy-loss experiments.

The movement of the conduction electrons of metals upon excitation with the incident light builds up polarisation charges on the metal particles. The polarisation charges create an electric field, which acts as restoring force in the system, allowing resonance to occur at a particular frequency of incident radiation. The resonant interaction between the surface charge oscillation and the electromagnetic field of light constitutes "surface plasmons", named by Stern and Ferrell [156].

Scientists have classified the "Surface Plasmons" in two categories: "Localised surface plasmons (LSP)" [157] and "Surface Plasmon Polaritons (SPP)" [141]. In the case of LSP, electromagnetic wave interacts with the metallic nanoparticles (such as Au, Ag, Pt, Pd) of diameter (d) much smaller than the incident wavelength (λ), i.e. $d << \lambda$. LSPs are confined in the closed surface of the nanoparticles and can be resonantly excited with the electromagnetic wave of particular frequency irrespective of the wave vector of the incident wave, which also leads to a strong amplification of the local electromagnetic field.

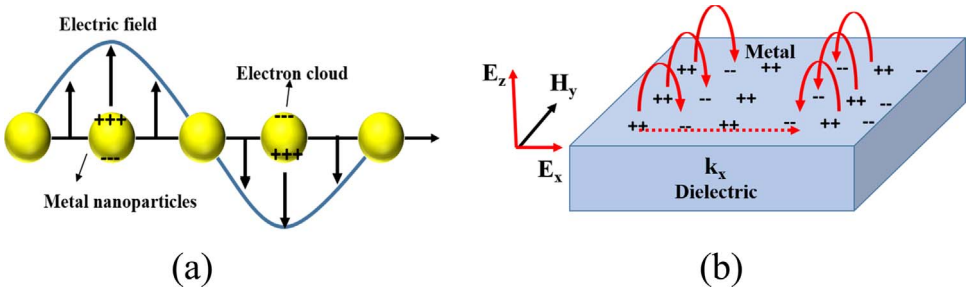

Fig. 7. : (a) Formation of localised surface plasmons (LSPs); (b) The propagation of surface plasmon polaritons (SPPs) in metal-dielectric interface in response to electro-magnetic field.

The frequency of LSPs are highly sensitive to the shape, size, size distribution, density, dielectric function of metal particles and surrounding environments.

In contrast, SPPs are the coherent collective oscillations of conductive electrons, confined at the interface of two media such as a metal and a dielectric. The SPPs propagate in a wavelike manner at the interface of the metal and dielectric perpendicular to the surface. The electromagnetic field of SPPs is evanescently confined in the boundary of metal-dielectric, which causes an enhancement of the electromagnetic field at the interface, leading to an extraordinary sensitivity of SPPs to surface conditions. The amplitude of the wave decays exponentially with an increase in distance from the interface due to the surface wave character of SPPs.

Fig. 7 demonstrates the fundamental difference between localised surface plasmons and surface plasmon polaritons. For LSPs, the electron cloud oscillates locally around the metallic nanoparticles, while the SPPs move in the x and y directions through the interface of metal and dielectric with an evanescent decay in the z direction. Therefore, both LSPs and SPPs manifest themselves in the enhancement of local filed.

Several theoretical and experimental investigations of SPPs have been performed to explore the fundamental properties of it and to continue a great variety of experiments in the field of condensed matter and surface physics [158]. SPPs are linked with a variety of distinctive phenomenon such as the energy transfer in gas-surface interactions, the energy loss of charged particle moving outside a metal surface and the damping of surface vibrational modes etc. The properties of SPPs have also been extensively utilised in a wide spectrum of studies ranging from electrochemistry [159], photonics [160], biosensing [161], optoelectronics [162], surface plasmon microscopy [163], surface plasmon resonance sensors [164], plasmonic lasers [165], light-emitting diodes [166] etc. However, here we limit ourselves in discussing the fundamentals of SPPs and its application in solar selective absorber coatings.

The discovery of SPPs has revealed a new regime in the development of solar selective absorber coatings. There are increasing number of excellent efforts on the development of solar selective absorber coating by using plasmonic enhancement with an aim to increase the efficiency of CSP systems. A thin film composed of DMD design is one of the most promising structures that can generate SPPs to achieve high solar selectivity as the film is transparent in the thermal infrared region, while they are strongly absorbing in the solar region. This structure is based on a thin metal film with low refractive index sandwiched by high refractive index dielectric films from both sides. The large refractive-index discontinuity at the boundary regions helps in subwavelength localisation and field enhancement effect. The combination of rapidly attenuating dielectrics and the noble metals results in a strong resonant behaviour in the thin film which leads to a considerable modifications of the optical properties in the selective coating.

Once incident sunlight is converted into SPP mode in DMD -based coatings, it will start to propagate. But the wave will gradually attenuate exponentially with increasing distance into each medium from the interface. The damping is caused primarily by dispersion near the resonant frequency [167], free-electron scattering in metal, and at short operating wavelengths by interband transitions. The large optical attenuation of SPPs also occurs due to the Joule losses ($Q = \int j.\, EdV$) in metal [167]. The roughness of the surface also causes additional attenuation. Moreover, the SPPs are scattered, while interacted with the surface defects. The destructive interference takes place between the scattered and the incoming light. All these phenomena reduce the overall reflections of the coating and increase absorption.

A complete theoretical treatment of SPPs is quite lengthy and beyond the scope of this review. However, we have attempted to provide the reader a limited overview on some equations related to SPPs in MD and DMD -based structures, their physical interpretations, and how these properties can be implemented in a solar selective absorber stack.

We have discussed earlier that the SPPs, a collective oscillation of conduction electrons in metal, can be generated at the interface of a metal and a dielectric material (see Fig. 8(a)). The SPP is transverse-magnetic (TM) wave that can be distinguished by the propagation

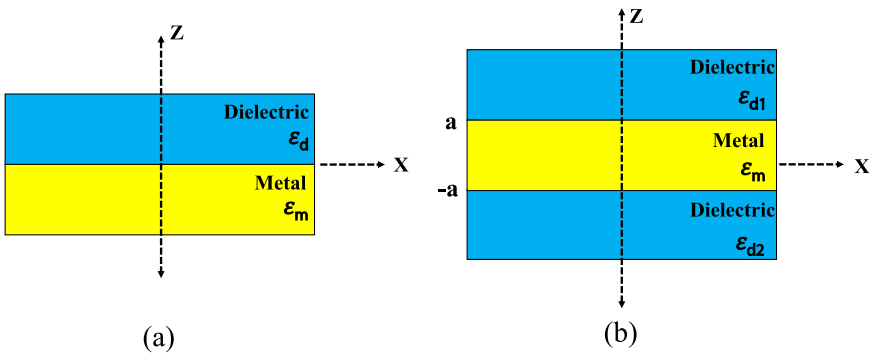

Fig. 8. : Schematic of the (a) metal-dielectric and (b) dielectric-metal-dielectric structures for SPP propagation.

constant and electromagnetic field distribution. The dispersion of the SPPs at the interface of metal with dielectric material can be calculated by solving Maxwell's equation in each medium.

While solving the Maxwell's equation, one need to ignore the following [168]:

(i) The metal and dielectric layers in real devices have a finite thickness,
(ii) There will be some initial absorption of light when it is propagating through the dielectric towards the interface,
(iii) Imperfect coupling of the incoming plane wave to SPPs takes place at the interface [169].

Bohn et al. [168] demonstrated that the analytical solution of the electric filed E_m (metal) and E_d (dielectric) which represents the SPP, can be obtained by the following equations:

$$E_m = \left[E_O,0,E_O\left(-\frac{k_x}{k_{z,m}}\right)\right]e^{i(k_x x+k_{z,m}z-\omega t)} \text{and} \tag{22}$$

$$E_d = \left[E_O,0,E_O\left(-\frac{k_x}{k_{z,m}}\right)\right]e^{i(k_x x-k_{z,m}z-\omega t)}, \tag{23}$$

where k_x is the wave vector parallel to the interface, and $k_{z,m}$ and $k_{z,d}$ are the wave vectors perpendicular to the interface in the metal and dielectric, respectively.

The solutions of the Maxwell's equations using appropriate boundary conditions represent the SPPs in MD structure. We can obtain the following dispersion relation of the SPP propagating in the interfaces between metal and dielectric [170]:

$$k_{SP} = k_O\sqrt{\frac{\varepsilon_d\varepsilon_m}{\varepsilon_d+\varepsilon_m}}, \tag{24}$$

where k_{SP} and k_o are the wave vector (momentum) of the SPPs and photon respectively, and ε_d and ε_m ($\varepsilon_m = \varepsilon_{mr} + i\varepsilon_{mi}$) are the frequency-dependent relative permittivities of the dielectric and metal, respectively.

The dissipative power of SPPs has been calculated using the Poynting Vector and power flow in the dielectric medium in a MD system. The power absorbed by the dielectric is presented by [168]:

$$\begin{aligned} P_{abs,d} &= \frac{1}{2}\int_0^\infty\int_0^\infty Re\{\sigma E_d E_d^*\}dxdz \\ &= \frac{\omega\varepsilon_O Im\{\varepsilon_d\}|E_O|^2}{8Im\{k_x\}Im\{k_{z,d}\}}\left(1+\frac{|\varepsilon_m|}{|\varepsilon_d|}\right). \end{aligned} \tag{25}$$

The power is not only be absorbed inside the dielectric but also in the metal. The ratio of the dissipative power in metal and dielectric can be expressed as

$$F_{abs} = \frac{P_{abs,d}}{P_{abs,m}} = \frac{Im\{\varepsilon_d\}|\varepsilon_m|Im\{k_{z,m}\}}{Im\{\varepsilon_m\}|\varepsilon_d|Im\{k_{z,d}\}}. \tag{26}$$

The ratio of the power absorbed in the dielectric to the total power absorbed by both metal and dielectric can be expressed in terms of F_{abs}:

$$\frac{P_{abs,d}}{P_{abs,d}+P_{abs,m}} = \frac{F_{abs}}{F_{abs}+1}. \tag{27}$$

In order to achieve maximum solar absorption in the meta-dielectric slab, the F_{abs} ratio should be maximized. Five independent variables are responsible to absorb maximum sunlight. These variables are the frequency of incoming photons, the real and imaginary permittivity for the metal, and the real and imaginary permittivity for the dielectric absorber. The highest absorption can be achieved in materials with small positive real permittivity and large positive imaginary permittivity. This is in view of the fact that the small real permittivity provides a large frequency range over which SPPs can be supported and, in practical devices, will reduce reflections at the interface between the external medium, such as air due to the smaller refractive index. On the other hand, the loss factor in a material can be defined by the following equation,

$$tan\delta = \frac{\varepsilon'^{'}}{\varepsilon'} \tag{28}$$

where tanδ is the loss factor; ε' and $\varepsilon'^{'}$ are the real and imaginary part of the relative permittivity, respectively [171]. Hence the second requirement for large imaginary permittivity or large extinction coefficient is necessary for the loss of the incident radiation in the system, which enhances the absorption. In order to fabricate an efficient metal-dielectric stack, we can also correlate the above mentioned criteria to the following equations;

$$n = \sqrt{\frac{\varepsilon'^2+\varepsilon'^{'2}}{2}+\frac{\varepsilon'}{2}} \tag{29}$$

$$k = \sqrt{\frac{\varepsilon'^2+\varepsilon'^{'2}}{2}-\frac{\varepsilon'}{2}} \tag{30}$$

where η and k are the real and imaginary part of the refractive index, respectively. The real and imaginary parts of two appropriate parameters such as refractive index and relative permittivity to evaluate the performance of any optical systems have been put together in the above equations. It is evident from Eqs. (29) and (30) that a lower value of real part of relative permittivity (ε') increases the imaginary refractive index which is responsible to boost the absorption of solar energy.

Now, let us consider a multilayer system of DMD, sketched in Fig. 8(b), consists of a thin metal films of thickness 2a and relative permittivity ε_m sandwiched between two optically semi-infinite dielectrics of relative permittivity ε_{d1} and ε_{d2} [172].

In this context, it is worthy to point out that the optical properties of a DMD -based system can be obtained by computational analysis of characteristic matrix theory [173]. Considering the incidence and the emission medium of the system is half-infinite and non-absorptive, one can represent the characteristic matric of dielectric-metal-dielectric as follows [174]:

$$\left\{\prod_{r=1}^{k}\begin{bmatrix} Cos\overline{\delta_r} & jSin\overline{\delta_r}/\overline{\eta_r} \\ j\overline{\eta_r}Sin\overline{\delta_r} & cos\overline{\delta_r}\end{bmatrix}\right\}\begin{bmatrix}1\\ \eta_{k+1}\end{bmatrix}$$

Therefore, the reflectance and the transmittance of the system can be expressed by

$$R = \left(\frac{\eta_O B - C}{\eta_O B + C}\right)\left(\frac{\eta_O B - C}{\eta_O B + C}\right)^* \text{and} \tag{31}$$

$$T = \frac{4\eta_O\eta_{k+1}}{(\eta_O B + C)(\eta_O B - C)}, \tag{32}$$

where $\overline{\delta_r}$ is the phase thickness and $\overline{\eta_r}$ is the complex admittance in the horizontal and vertical directions. B, C, $\overline{\delta_r}$ and $\overline{\eta_r}$ can be calculated using complex refractive index and variable thickness of the materials along with wavelength of the incident light. The value of the refractive index can also be found from data in Palik's handbook [175], or from earlier data derived by Johnson and Christy [176]. Different commercial software such as The Essential Macleod, Thin film Centre, Inc etc., are used to find the reflectance, absorptance and transmittance from the characteristics matrix.

The optical properties of the DMD system can also be evaluated using dispersion relation of the SPPs in each optically homogeneous, isotropic, linear media without any influence of external charge or and current densities. The continuity of electric and magnetic field leads to the following dispersion relation of DMD system [172]:

$$e^{-4k_m a} = \frac{\frac{k_m}{\epsilon_m} + \frac{k_{d1}}{\epsilon_{d1}}}{\frac{k_m}{\epsilon_m} - \frac{k_{d1}}{\epsilon_{d1}}} \cdot \frac{\frac{k_m}{\epsilon_m} + \frac{k_{d2}}{\epsilon_{d2}}}{\frac{k_m}{\epsilon_m} - \frac{k_{d2}}{\epsilon_{d2}}} \quad (33)$$

It is noteworthy that the SPPs can be excited in visible wavelength range while the magnitude of the real component of the metal's dielectric constant becomes larger than the corresponding (positive) value for the dielectric. In DMD structure, the incident sunlight is turned by 90° and the solar radiation is confined in the horizontal direction of the selective coating. In this case, the length of the solar selective absorber coating should be greater than optical absorption length. Depending on the properties of the metal and dielectric, SPP possesses high loss in different wavelength regime. The decay of evanescent waves occur in both metal and dielectric. However, to enhance the solar selectivity of the absorber coating, the decay of evanescent wave in dielectric is more important than in metal. Maximization of absorption can be ensured by increasing the decay length of the evanescent wave [177].

An alternative method for depicting the solar absorption in DMD structure is through the local density of optical states ρ(r, ω), which is a function of position r and radial frequency ω. ω can be determined from the local density of electromagnetic energy, which can be expressed as

$$U(r,\omega) = \frac{\rho(r,\omega)h\omega}{e^{\frac{h\omega}{k_B T}} - 1}, \quad (34)$$

where hω and $k_B T$ are photon energy and thermal energy, respectively. The local density of optical states increases in the interface of metal and dielectric due to the presence of additional evanescent modes. As a result, trapping of solar energy can be enhanced significantly in the DMD structure. The trapping in the structure raises the macroscopic limit of $4\eta_d^2$ by a factor of $\left(\frac{2\eta_d}{\eta_m} + \frac{\eta_d^5}{\eta_m^5}\right)/3$, which equals 12 when η_d/η_m is equal to 2 [106].

In case of DMD structure, the fractional absorption in the dielectric layer can be represented as:

$$f_d = \frac{k_d k_m^3}{\eta_d^3 \eta_m + k_d k_m^3} \quad (35)$$

where η_d (η_m) and k_d (k_m) are the real and imaginary parts of the refractive index of dielectric (metal). The half of the energy will be absorbed in the dielectric if $k_s > \frac{\eta_m \eta_d^3}{k_m^3}$. A small value of η_m/k_m^3 will enhance the absorption in dielectric layer drastically.

It is worthwhile to mention that refractive index of two dielectric layer in the DMD structure should be equal or close enough to allow the effective coupling of the SP waves. Hence, in order to improve the solar selectivity in DMD -based coatings, the main approach is to use highly absorbing dielectrics where sunlight will be effectively attenuated along with a metal that have finite optical conductivity. The large optical attenuation in the highly absorbing dielectric and the infrared reflectivity of the metal give access to high solar absorptance in solar spectrum and low thermal emittance in the infrared regime.

6. Dielectric-metal-dielectric based solar selective absorbers: case studies

6.1. $Cr_xO_y/Cr/Cr_2O_3$

Chromium (III) oxide is an important refractory material which has been widely studied in various field over last several decades. Its high melting point (~ 2435 °C) [178], superior hardness [179], low friction, oxidation and corrosion resistance [180] make it one of the choice for using as a superior protective coating. It also has been utilised as an intermediate layer in corrosion-resistant applications on semi-conductors [181] and metals, an active tunnelling barrier or pinning system for spintronic applications [182]. The attractive optical properties of chromium oxide enable it to use as a pigment powder with high NIR reflectance [183], attenuated phase-shifting masks for deep ultraviolet (UV) lithography. Being thermally stable [184], Cr_2O_3 has a fundamental and practical importance in the UV, visible, and IR regions of the electromagnetic spectrum, Cr - Cr_2O_3-based cermet coatings have been well exploited for photothermal applications [185]. Excellent solar selectivity with a high solar absorptance and low emittance have been obtained from these coatings over a large temperature range. Recently, most of the Cr - Cr_2O_3 solar selective coatings are deposited by reactive direct current (dc) and radio frequency (rf) sputtering technique [110,186,187]. The difficulty in the formation of the oxide and the low growth rates limit the use of dc and rf sputtering in depositing Cr-Cr_2O_3 coating [188].

In response to the growing demand for the industrial use of Cr_2O_3 or black chrome [189,190] in the field of solar selective coating, Barshilia et al. [152] first investigated the feasibility of depositing $Cr_xOy/Cr/Cr_2O_3$ -based coating using asymmetric bipolar-pulsed dc generators. They found that $Cr_xO_y/Cr/Cr_2O_3$ (thickness - 28 nm/ 13 nm/64 nm) has a very high selectivity with an absorptance of 0.899–0.912 and a low emittance of 0.05 – 0.06. The agreement with experimental ellipsometric data with the theoretical models confirms that Cr_xO_y and Cr layers act as main absorber layers, while top Cr_2O_3 serves the role of antireflection coating. The refractive index and extinction coefficient of the layers were explored using Adachi's model for Cr_xO_y and Cr_2O_3 layers while Cauchy's model was used for Cr layer. X-ray diffraction study indicated the amorphous nature of the coating. XPS investigations showed that the state of chromium was in the form of Cr^{3+}. They have also studied the thermal stability of the coating in the range of 200–400 °C for 2 h. They showed that there was no significant change in absorptance, emittance and surface roughness after heat treatment up to 300 °C. At higher temperatures, selective performance degraded drastically due to oxidation of Cr. The XPS and micro-Raman spectroscopy also reveal that Cr metal content was responsible for absorption of solar energy in Cr_2O_3 matrix. As Cr atoms turn into Cr_2O_3 at high temperature, the absorptance decreases. The emittance also increases because of the sudden rise in surface roughness (> 142 nm) of the coating. Not only that, the diffusion of Cu atoms towards the coating leads to form CuO and $CuCr_2O_4$. Moreover, the differences in thermal expansion coefficient of Cu, Cr and Cr_2O_3 also results the degradation of optical properties and delamination of coating. The coating was shown to be stable for 250 h at 250 °C in air with an absorptance and emittance of 0.898/0.11. However, the coating was thermally stable up to 500 °C while heat treated in vacuum. When the annealing temperature reaches more than 500 °C, the absorptance decreases. They also calculated the activation energy required for the degradation using Arrhenius equation which can be presented by the following equation.

$$\ln(\Delta\alpha) = \frac{E_a}{RT} + constant \quad (36)$$

where Δα is change in absorptance while heat treated at temperature T and R is the universal constant. The activation energy of this coating came out to be 100 kJ/mol using the slope of the ln (Δα) vs 1000/T plot (Fig. 9.) i.e. Arrhenius plot for five temperatures (200, 250, 300, 325, 350 °C) for longer and 2 hrs durations. However, this study not only demonstrates the fabrication of a novel coating but also addresses the improvements in thermal performance comparison with Cr - Cr_2O_3 – based coating.

6.2. MgO/Zr/MgO

Magnesium oxide with the rock salt structure [191] has become one of the most representative materials among the oxides due to its wide band gap (7.8 eV), good thermal conductivity [192], an excellent chemical and thermal stability (melting point 2800 °C) [193]. These

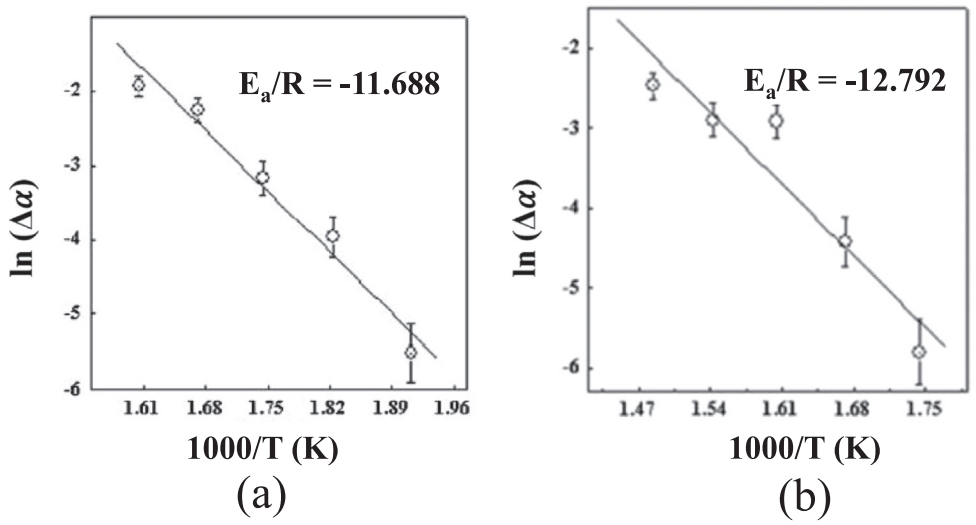

Fig. 9. The Arrhenious plot for $Cr_xO_y/Cr/Cr_2O_3$ coatings [152].

properties enable it to be used in ceramic construction of thermocouples and energy converters [194], thermal shock transducers for electrical insulation [195] and in AC plasma display panel for protecting layer [196]. Not only that, considerable interest has been shown in the use of MgO as a buffer layer for high-temperature superconductor applications [197]. Based on the outstanding properties of MgO, it has been chosen as a suitable material for high temperature solar selective absorber coating.

Maziere-Bezes et al. [198] first developed Au–MgO solar selective cermet by DC reactive sputtering, and they concluded that a high metallic volume fraction (f ≥0.35) is required to absorb solar radiation. Motivated with this, Nuru et al. [199] fabricated MgO/Zr/MgO –based solar selective coating on Zr-coated SS substrate. The absorptance of the film was found to be 0.92 and the emittance was 0.09. They found that the selective coating formed a banana like columnar structure with an average column length of 17.02 ± 0.15 nm, as revealed from AFM image (shown in Fig. 10(a)). They also measured the reflectance spectra using SCOUT software by fitting the dielectric constant and the thickness of the coating, Fig. 10(b) indicates that calculated and the measured reflectance spectra matches exactly. The coating exhibited less than 25% reflectance up to a wavelength of 1200 nm and after that the reflectance of the coating increases. The thickness of individual layer of the MgO/Zr/MgO/Zr coating was found to be 92.6, 10, 78.3 and 74.8 nm from surface to substrate.

The coating also exhibited high thermal stability up to 400 °C for 2 h in vacuum with a high absorptance of 0.918 and low emittance of 0.10. The absorptance of the coating reduced to 0.893 and thermal emittance increased to 0.12 when heat treated at 500 °C in vacuum. In a separate study, they investigated the thermal stability of the coating in air [200], and was observed that the coating shows efficient performance up to 300 °C in air (α=0.91; ε=0.12). The efficiency of the coating decreased, while heat treated at 400 °C for 2 hrs (α=0.85; ε=0.14). They performed the heavy Ion ERDA measurement to investigate the reason behind the degradation of the coating and concluded that the loss of oxygen at the surface and an increase in the oxygen content at the Zr base layer/substrate interface caused the failure of the coating. The oxygen content in MgO on top surface decreases due to thermal stress. As a result the metal component of MgO layer, i.e. Mg, a highly reflecting metal, affected the absorptance of the coating. Moreover, the formation of ZrO_2 due to oxidation of Zr metal changed the configuration of the coating from MgO/Zr/MgO to MgO-ZrO_2 matrix. The two transparent dielectric in the coating did not help to absorb the solar energy, and most of the portion of the solar spectrum transmitted through the layer. On the other hand, the metallic interlayer of Zr, no more worked as infrared reflector due to the formation of ZrO_2 and consequently the emittance increased.

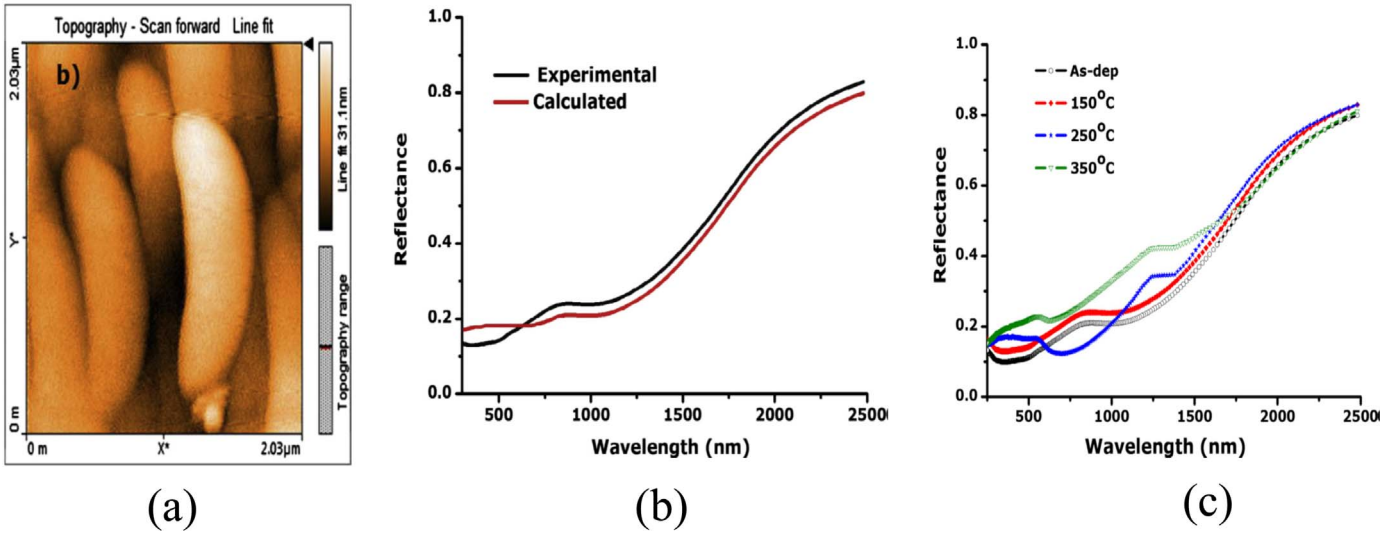

Fig. 10. (a) AFM images (b) Experimental and calculated reflectance spectra and (c) thermal stability of MgO/Zr/MgO coating [199,200].

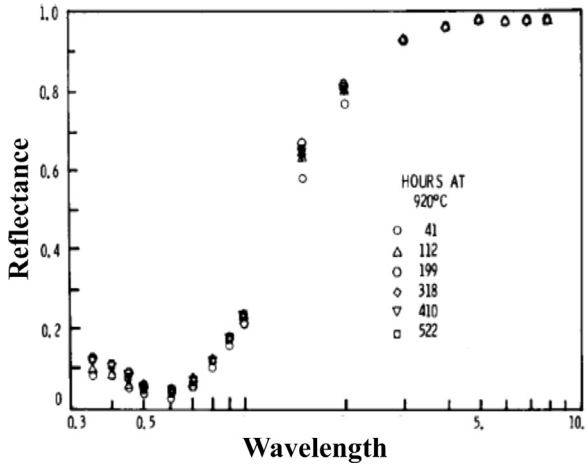

Fig. 11. Spectra reflectance of $Al_2O_3/Mo/Al_2O_3$ coating after long term annealing at 920 °C [207].

However, as far as the long-term stability of the coating is concerned, the coating exhibited thermal stability up to 250 °C for 24 hrs. The thermal stability of MgO/Zr/MgO coating have been presented in Fig. 10(c).

6.3. $Al_2O_3/Mo/Al_2O_3$

A large number of Al_2O_3 -based cermet coatings such as Ni-Al_2O_3 [201], Mo-Al_2O_3 [118], Au-Al_2O_3 [202] , Ag-Al_2O_3 [116], W-Al_2O_3 [114], Co-Al_2O_3 [203], Fe-Al_2O_3 [204] and Pt-Al_2O_3 [205] have shown promising selective properties. However, the structure with a metallic layer (Ni, Mo, Al) in between two Al_2O_3 layers have become a versatile and potential structure for successful use as selective coatings in solar thermal system.

Schmidt and Park [206] engineered an attractive design of absorber coating consisting of multiple alternate layer of Mo and Al_2O_3, and fabricated it using electron beam evaporation technique. $Al_2O_3/Mo/Al_2O_3/Mo/Al_2O_3/Mo/Al_2O_3/Mo$ –based absorber coating on Mo substrate exhibits high absorptance and emittance of 0.91 and 0.085 at 260 °C in vacuum. The emittance value recorded was 0.16 at 538 °C. Another $Al_2O_3/Mo/Al_2O_3$ coating on Mo substrate was prepared by Peterson and Ramsey [207], which showed exotic thermal resistance by withstanding 10,000 cycles between 820 and 860 °C. This absorber satisfied a reasonable goal of selectivity with absorptance of 85% and thermal emittance of 11% and 22% in 500 °C and 1000 °C respectively.

As shown in Fig. 11, there is no change in the reflectance spectra even if after heating the sample beyond 500 hrs at 920 °C, which signified extremely good thermal stability of coating. In order to reduce the cost of the entire stack, they replaced the expensive Mo substrate by a Mo coated (thickness 3000–6000 Å) stainless steel substrate and studied the thermal stability in vacuum for 1 h. They found that coating on Mo substrate was stable up to ~ 1050 °C while the coating deposited on stainless steel substrate started degrading at ~ 900 °C due to diffusion of Fe and Cr atoms from substrates to the $Al_2O_3/Mo/Al_2O_3$ coating. Lifetime of both the coating was estimated using high temperature results. The estimation indicated that the coating on Mo substrate can survive more than 20 years at 800 °C, whereas a longer life time at 400 °C is expected for the coating on Mo coated stainless steel substrate. However, the high temperature stability of the coating in air is lacking in their study.

John et al. [208] prepared $Al_2O_3/Mo/Al_2O_3$ coating by cylindrical magnetron sputtering onto a Mo coated glass and stainless steel substrates. The thickness of the infrared reflector and the diffusion barrier of Mo layer on both the substrates was 80 nm. They prepared different types of coating by varying the deposition condition (Ar environment, i.e., without presence of O_2 and in Ar + O_2 environment, i.e., with presence of O_2) of the intermediate metallic Mo layer, sandwiched between two Al_2O_3 layers. The Mo layer, deposited in the Ar environment is indicated by $Al_2O_3/Mo/Al_2O_3$, while the latter is denoted by $Al_2O_3/Mo(O)/Al_2O_3$. $Al_2O_3/Mo/Al_2O_3$ coating exhibited hemispherical absorptance and emittance of 0.90 ~ 0.92 and 0.08, respectively whereas $Al_2O_3/Mo(O)/Al_2O_3$ exhibited 0.94 ~ 0.95 and 0.06 – 0.07. It can also be noted that the optimized thickness for $Al_2O_3/Mo/Al_2O_3$ and $Al_2O_3/Mo(O)/Al_2O_3$ with the highest achievable optical properties are 70 nm/8 nm/70 nm and 90 nm/20 nm/50 nm, respectively. The presence of oxygen in the middle layer i.e. in Mo(O) layer changes the selectivity of multi-layer in such a way so that the coating could not possess selectivity with the optimized thickness of $Al_2O_3/Mo/Al_2O_3$ stack and there was a need of repetitive optimization of thickness for $Al_2O_3/Mo(O)/Al_2O_3$ coating . Hence it is clear from the study that a small change in the composition of the individual layer can drastically change the entire property as well as other optimized parameter of the stack. One of the major focus of the study was on to the optical properties of the coating, represented in Fig. 12(a), which clearly showed that the refractive index and extinction coefficient of Mo(O) layer is significantly lesser in the long wavelength in comparison to those of Mo layer, and this was considered the reason for the low emittance of $Al_2O_3/Mo(O)/Al_2O_3$ coating.

The Al_2O_3 layers were fabricated using two different types of targets, such as reactive sputtering from Al and r.f. sputtering from

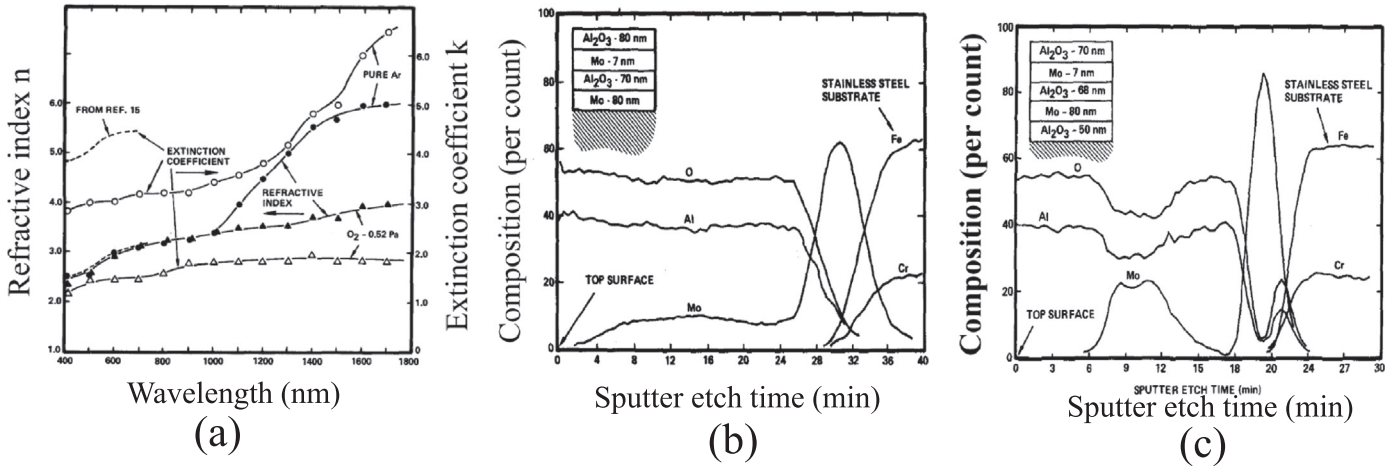

Fig. 12. The wavelength dependence of refractive index and extinction coefficient of Mo films, sputtered in pure Ar and in an Ar + O_2 mixture; Auger depth profile-composition analysis of heat-treated $Al_2O_3/Mo/Al_2O_3$ coating in vacuum, deposited on Mo coated stainless steel substrate a) Al_2O_3 layer deposited by reactive sputtering; (b) Al_2O_3 layer deposited by r.f sputtering of alumina [208].

Al_2O_3 targets. The coatings with reactively sputtered Al_2O_3 layers were thermally stable at 300 °C in air and 400 °C in vacuum. After heat treatment of the coating at 500 °C in vacuum, the distinct Mo layer was completely intermixed with Al_2O_3 layer, which was obtained from Augur depth profile study, presented in Fig. 12(b). On the other hand, the coatings with direct r.f sputtered Al_2O_3 appeared to be stable up to 700 °C in vacuum (see Fig. 12(c)). In this case, it was observed that though chromium and iron have diffused from stainless steel surface, they were strongly restrained by Al_2O_3 and there was no intermixing between Mo and Al_2O_3 layers. Hence, the solar selectivity was not affected in high temperature. They concluded that direct r.f sputtered Al_2O_3 provides a superior diffusion barrier. Therefore, it can be stated from these observations that the high temperatures stability of the DMD stack not only depends on the materials but also the method used for deposition. One of the interesting achievement of the study was to use a dielectric layer (r.f. sputtered Al_2O_3 of thickness 50 nm) as a diffusion barrier instead of a metal. The metallic layers as the infrared reflector and diffusion barrier in such coatings are highly appreciated by the scientific community [209,210]. However, surprisingly Al_2O_3 coating as a diffusion barrier on the stainless steel surface thermally protected Al_2O_3/Mo/Al_2O_3/Mo coating on Al_2O_3 coated stainless steel substrate in air at 550 °C after 14 hrs without any change in the optical properties.

In a separate study, they fabricated Al_2O_3/M/Al_2O_3/R coatings where M is a semi-transparent absorbing layer and R is a low emittance reflecting layer [211]. The M layers could be different metals, such as Cr, Ni, Mo, Ta. The R layer was of same metal as the M layer. Alike the previous work, they used direct r.f sputtering and reactive sputtering to prepare Al_2O_3 layers. The multilayer absorber coatings were heat-treated in air and vacuum over the temperature range of 300–700 °C for periods from 8 to about 1000 h. The results of the thermal stability, presented in Table 1, are in good agreement with the previous findings [208] on cylindrical-magnetron-sputtered Al_2O_3/Mo/A1$2O_3$ coatings. The coating with r.f sputtered Al_2O_3 layer showed better performance than reactively sputtered Al_2O_3. Hence, it can be confirmed that the deposition procedure is a crucial parameter to improve the thermal stability of CSP systems.

Table 1
Thermal stability of Al_2O_3/M/Al_2O_3/R coating in air and vacuum [211].

Coatings	Thermal stability			
	air		vacuum	
	Stable (°C)	Failure (°C)	Stable (°C)	Failure (°C)
M ≡ Cr ; R ≡ Cr Reactively sputtered Al_2O_3, Cold	___	300	___	350–400
R.f sputtered Al_2O_3, Cold	450	500		
R.f sputtered Al_2O_3, hot	500	550	650 – 700	___
M ≡ Mo; R ≡ Mo Reactively sputtered Al_2O_3, Cold	400	400–450	400	450–500
Reactively sputtered Al_2O_3, hot	500	___		
R.f sputtered Al_2O_3, Cold	500–550	___		
R.f sputtered Al_2O_3, hot	500–550	___	650–700	___
M ≡ Ni; R ≡ NiReactively sputtered Al_2O_3, Cold	350	400	400	450
Reactively sputtered Al_2O_3, hot	400	400–500		
R.f sputtered Al_2O_3, Cold	400	450		
R.f sputtered Al_2O_3, hot	500	550	650 – 700	___
M = Ta; R = Ta Reactively sputtered Al_2O_3, Cold	___	350		

6.4. $Al_xO_y/Al/Al_xO_y$

A well-known example of a DMD absorber is $Al_xOy/Al/Al_xO_y$, which has been developed by Barshilia et al. [149] on Cu and Mo substrates using asymmetric bipolar- pulsed DC generators for high-temperature applications. The optimized absorber, with a total thickness of 150–170 nm (97 nm of Al_xO_y anti-reflection layer, 15 nm of metallic Al layer and 40 nm of absorber Al_xO_y layer) had a solar absorptance of 0.950–0.970 and thermal emittance of 0.05–0.08. The spectroscopic ellipsometry was used to find out the refractive index and the extinction co-efficient of the individual layer. The ellipsometric data was fitted by Drude's and Tauc Lorentz model, and the fitting confirms the metallic and the dielectric nature of Al and Al_xO_y layers, respectively. Fig. 13 indicates the variation of refractive index (n) and extinction co-efficient (k) with respect to wavelength of Al and Al_xO_y layers. The ellipsometry results reveal the same value of n and k for top and bottom Al_xO_y layers. The n value of Al_xO_y layer decreases with an increase in wavelength while k value was zero in the whole wavelength range, representing dielectric nature of Al_xO_y [174]. In contrast, there was an increase of n and k value throughout the whole wavelength range for Al, indicating the metallic behaviour of Al. The heat treatment of the coating, deposited on Cu substrate, was carried out in different temperatures for 2 hrs to evaluate the thermal stability. The annealing upto 400 °C in air did not affect the selective property ($\alpha/\varepsilon \sim 0.901/0.06$) of the coating. The spectral and structural degradation was found at T > 450 °C ($\alpha/\varepsilon \sim 0.790/0.07$). The structural delamination was confirmed by the Raman spectroscopy in Fig. 14. Two Raman peaks of CuO at 211 and 291 cm^{-1} are an indication of outward diffusion of Cu substrate. However, they found different reasons behind the degradation of optical properties at high temperature, such as oxidation of Cu substrate, formation of $CuAl_2O_4$ compound due to intermixing of Cu and Al in high temperature, the transformation of nanocrystalline Al to metastable aluminium oxide, and differences in thermal expansion coeffiecnt of Al (24×10^{-6}/°C), Al_2O_3 (8.1×10^{-6}/°C) and Cu (16.5×10^{-6}/°C) substrates.

Thermal stability of the coating deposited on Mo substrate in vacuum was also investigated. After annealing at 800 °C for 2 h in vacuum, though the solar absorptance decrease, thermal emittance of the coating also decreased ($\Delta\alpha = -0.004$; $\Delta\varepsilon = -0.04$). The solar absorptance decreased and thermal emittance increased a lot when heat treated at 900 °C ($\Delta\alpha = -0.246$, $\Delta\varepsilon = 0.004$). Accelerated aging test of the coating on Cu substrate suggested that the coating was efficient even after heat treatment up to 200 and 75 h at 250 ($\Delta\alpha = -0.022$; $\Delta\varepsilon = 0$) and 300 °C ($\Delta\alpha = -0.031$; $\Delta\varepsilon = 0$), respectively. A performance criterion function (PC) for domestic hot water system has been defined by the International Energy Agency Solar Heating and Cooling Program (IEASHC) Task X,

$$PC = -\Delta\alpha + 0.25\Delta\varepsilon < 0.05 \quad (37)$$

The change in the absorptance and emittance after performing the accelerated aging tests confirmed service life time of at least 25 years for $Al_xO_y/Al/Al_xO_y$ coating. They have also calculated the activation energy for the degradation of the multilayer stack using Arrhenius equation (Eq. (36)), and determined it to be 64 KJ/mole.

6.5. $Al_xO_y/Pt/Al_xO_y$

Despite the fact that Pt is expensive, the good electrical conductivity, unreactive chemical behaviour and corrosion resistance of Pt made it one of the choices for the metallic layer of $Al_xO_y/Pt/Al_xO_y$ stack. Nuru et al. reported a series of observations [209,212–216] on $Al_xO_y/Pt/Al_xO_y$ stack. In one of their studies [212], they used electron beam evaporation technique to successfully deposit the coating onto 1737 corning glass, silicon (111) and copper substrates. They also demonstrated that the thickness is a very important criterion to be a selective absorber coating. They have noticed a decrease in the refractive index

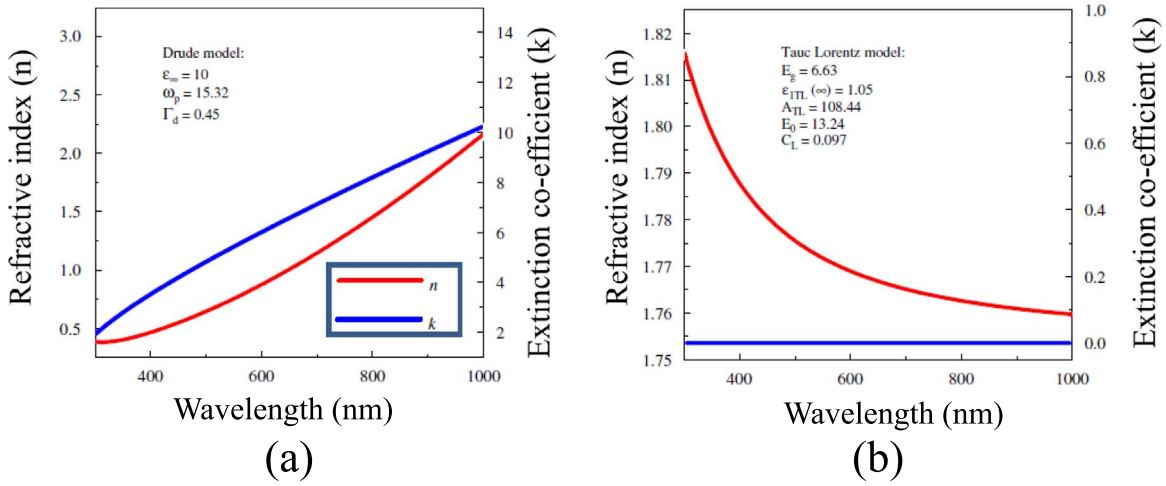

Fig. 13. Dependence of experimentally determined n and k values with respect to wavelength for (a) Al_xO_y (layers 1 and 3) (b) Al layer in Al_xO_y/Al/Al_xO_y absorber coating deposited on Cu substrate [149].

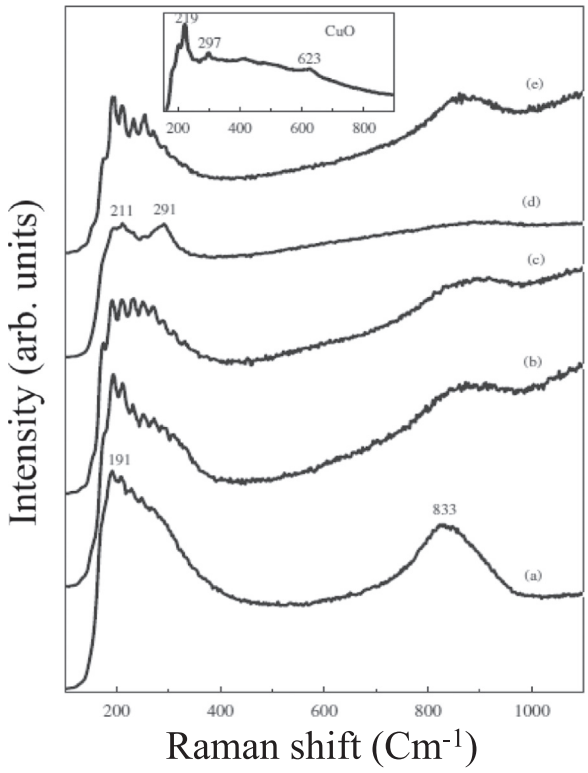

Fig. 14. Raman spectra of (a) as-deposited and heat treated absorbers annealed in air at (b) 250 °C, (c) 350 °C, (d) 450 °C and (e) 500 °C for 2 h in vacuum. The Raman spectrum of CuO has been represented in the inset [149].

of top and bottom Al_xO_y layer with a decrease in the thickness and increase in wavelength (Fig. 15(a) & (b)). However, the extinction coefficient remains unchanged with a constant value of zero in overall wavelength range, suggesting the dielectric behaviour of Al_xO_y layer. In contrary, the refractive index of Pt layer increases with increasing wavelength and thickness, while extinction co-efficient decreases with an increase in thickness which confirms the semi-transparent nature of Pt metal {see Figs. 15(c) and (d)}. Moreover, the refractive index of the top AlxOy layer is lesser than that of Pt layer revealing the anti-reflection property of the top Al_xO_y layer. They have also investigated the change in the reflectance spectra by varying the thickness of individual layer. They found that an increase of top Al_xO_y layer thickness leads to high reflectance in visible region along with a shift to higher wavelengths. In addition, more number of interference peaks appeared in the visible region. The thicker Al_xO_y layer (900 Å) helped to absorb more sunlight by shifting the reflectance spectra towards higher wavelength side, which can be seen in Fig. 16(a). For base Al_xO_y layer, the reflectance decreases monotonically with an increase in thickness from 100 to 400 Å, and an interference peak is observed in the lower wavelength regime at the thickness of 500 and 600 Å in Fig. 16(b). The optimized thickness was found to be 900 Å for the Al_xO_y top layer, 70 Å for the middle Pt layer and 400 Å for the base Al_xO_y layer to achieve highest selectivity. They determined the thickness using the Rutherford backscattering spectrometer (RBS). The coating exhibited a high solar absorptance of $\alpha = 0.94 \pm 0.01$ and thermal emittance of $\varepsilon = 0.06 \pm 0.01$. XRD study suggested the amorphous nature of Al_xO_y while the SEM study showed that flake like morphology of the multilayer stack consists of the Pt nano particles with an average diameter and interparticles distance of 146 and 6–10 nm, in and between the rims of Al_xO_y [213]. The surface roughness (6.5 ± 0.13 nm) of the stack was found to be comparable to the interparticle distance. The optical constants (refractive index and extinction coefficient) were measured to confirm the metallic and dielectric property of Pt and Al_2O_3, respectively, in different thickness by ellipsometry measurements. Using the optical constants for different thicknesses as input, the reflectance spectra of the multilayer was computed in an optical spectrum simulation program SCOUT. The simulated and the experimental reflectance spectra of the coating shown in Fig. 16(c) are in good agreement with each other. The absorptance and emittance value along with the reflectance spectra confirms the potential of Al_xO_y/Pt/Al_xO_y as good absorber.

The heat treatment of the coating shows that the coating is thermally stable up to 500 °C in air with solar selectivity 0.951/0.09 [214]. The SEM images of the coating, shown in Fig. 17 suggests that the size of the Pt nanopartilces increases with temperature and the particles agglomerate at the temperature more than 500 °C. As a result, the surface roughness of the coating also increases. The agglomeration of Pt particle and formation of CuO and Cu_2O due to surface diffusion leads to degradation of the selective property of the coating (0.846/0.11). The high temperature heat treatment also caused a decrease in the constituents of the absorber coating, which was confirmed by heavy ion elastic recoil detection analysis [215]. The reflectance spectra of the coating, heat treated at 600 and 700 °C in Fig. 18(a) shows a huge deviation from that of as-deposited coating. However, long temperature stability study showed that the coating is stable up to 450 °C in air for 24 h (see Fig. 18 (b)).

To improve the thermal stability further in a separate study, Nuru et al. [209] used Tantalum layer as a diffusion barrier on top of copper substrate. The incorporation of Ta layer increased the stability of the

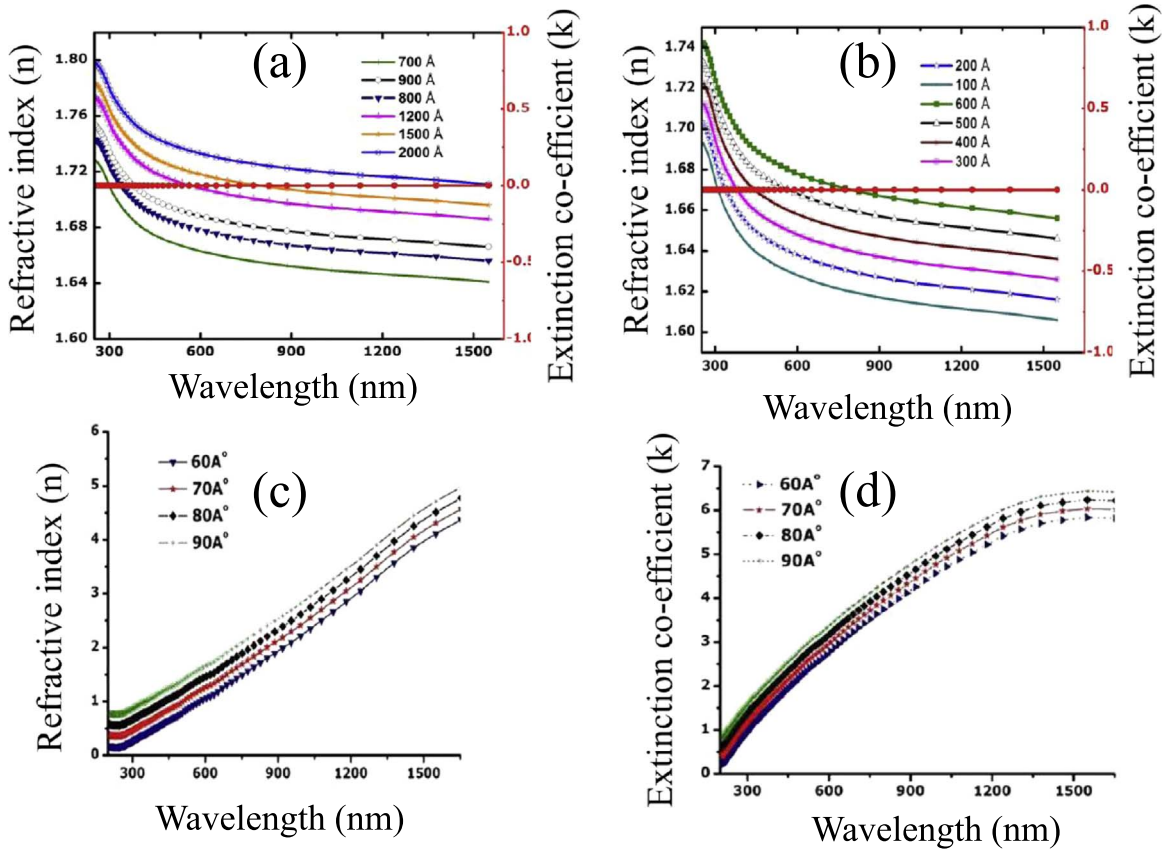

Fig. 15. The variation of optical constants as a function of wavelength in difference thickness of (a) top Al_xO_y layer, (b) base Al_xO_y layer (c) and (d) [212].

coating up to 700 °C for 2 h and the coating showed superior selectivity with absorptance of 0.932 and emittance of 0.10. When the long term thermal stability experiment was performed they found that the Ta/Al_xO_y/Pt/Al_xO_y is stable upto 550 °C for 24 h.

In a separate study, Nuru et al. [216] studied the effect of substrate temperature on selective property of e-beam evaporated Al_xO_y/Pt/Al_xO_y coating . They have observed that the particle size and the roughness of the coating increase when the substrate temperature has been changed from room temperature to 50, 100, 150 and 250 °C. The reason behind this can be attributed to the distant migration of the atoms which causes formation of denser grains and larger particles. As a result the solar absorptance of the coating decreases and the reflectance spectra shift towards shorter wavelength. Hence, it is evident from the study that substrate temperature during deposition is also a prime factor to reach the spectral selectivity.

6.6. $Al_xO_y/Ni/Al_xO_y$

Tsai et al. [217] proposed that the configuration of three layer coatings consists of a metal Ni layer in between two Al_xO_y layer. The Al_xO_y/Ni/Al_xO_y coating was deposited on a stainless-steel substrate using reactive DC magnetron sputtering. They investigated a group of samples to study the influence of target power and oxygen flow in the structure, surface morphology and chemical composition of the film. The Al_xO_y coatings deposited using various DC powers and oxygen flow rates are represented as A (DC power/oxygen flow rate). The transmission electron microscopy images in Fig. 19(a), (b) and (c) suggest that the coating deposited with lower oxygen flow rate (2 sccm) are loose and the surface of the coatings were rough, whereas the coating prepared in higher oxygen flow rate (8 sccm) appears to be very dense and the film surface is also very smooth. In addition, they observed that the film surface had become looser and rougher with an increase in target power from 150 W to 250 W. An increase in sputtering power and decrease in oxygen flow rates result an increase in Al_xO_y deposition rate. Therefore, the reason behind the difference surface morphology and density of the film may be caused due to difference in the deposition rates.

In addition, XRD study showed that the structure of all the coatings were amorphous as the crystallization temperature of Al_2O_3 is more than 900 °C. The diffraction pattern in Fig. 19(d), obtained from transmission electron microscopy is also in good agreement with the XRD study. The transmission spectra of the coating in Fig. 20 suggested that the loose coating with voids showed less transmission than the dense coatings, which indicates the voids and loose pattern helps in increasing the light absorption.

They also investigated the effect of different thickness in the optical properties of the coatings. To satisfy the criterion of destructive interference for light absorption, the optical thickness, i.e. (refractive index × film thickness) of the coating, should be quarter of incident wavelength. The thickness of the top layers were kept at 90 nm, 70 nm and 40 nm. The coating SS/Al_xO_y (70 nm)/Ni (20 nm)/Al_xO_y (70 nm) exhibited highest selectivity among all other coatings with an absorptance of 0.932 and emittance of 0.038. The coating, deposited in the operating condition of 150 W power and 8 sccm O_2 flow, exhibited thermal stability at least up to 12 h at 400 °C.

6.7. $HfO_x/Mo/HfO_2$

Different properties of hafnium oxide (HfO_2) are being currently investigated with great interest in various applications such as semiconductor devices [218], electronics [219], thermal barrier for turbine blades [220], high power lasers [221], waveguides [222] etc, due to its high dielectric constant (k ~ 25) [223], wide band gap (E_g ~ 5.8 eV) [224], high refractive index (1.85–2.15) [225,226], transparency over a

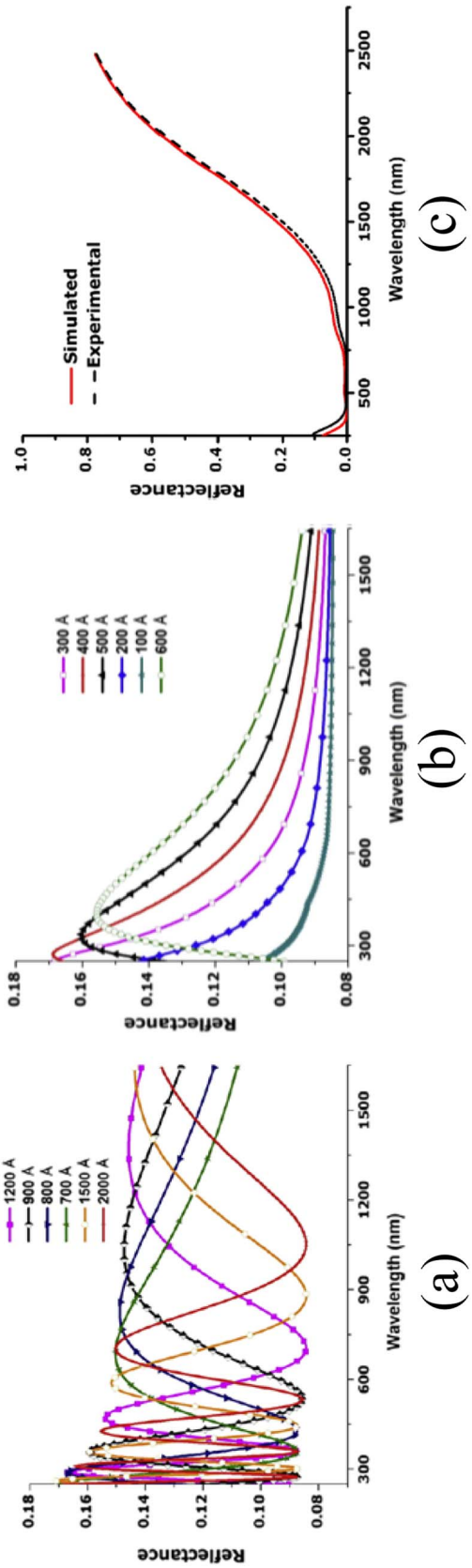

Fig. 16. The thickness dependence of reflectance spectra (a) top Al_xO_y layer (b) base Al_xO_y layer and (c) simulated and experimental spectra of Al_xO_y-Pt-Al_xO_y absorber coating [212].

wide range of wavelength, extending from UV (200 nm) to near-IR range (1.2 μm) [227], low chemical reactivity and high structural stability [228], excellent thermal stability [229], good abrasion/scratch resistance and hardness [230]. The HfO_2 coating have also been explored in various optical applications like anti-reflection coating [231], UV mirrors with a high damage threshold [232], optical filters [233], heat-mirrors in energy-efficient windows [234], astronomically charged couple devices [235] etc., because of anti-reflection property, high reflectance in IR region, high melting point (2800 °C) [229] and the hydrophobic property of HfO_2 [236].

Barshilia et al. [153] explored $HfO_x/Mo/HfO_2$ as a promising solar selective absorber coatings. Unlike other DMD film, the top stoichiometric HfO_2 layer allows the sunlight to reach to MO surface, whereas non stoitiometric HfO_x layer helps to absorb solar radiation. The coating was deposited on Cu and SS substrate using a DC unbalanced magnetron sputtering. Optimized film on Cu substrate exhibited high absorptance (0.905–0.923) and a low thermal emittance (0.07–0.09), while films on SS substrate had absorptance of ~ 0.902–0.917 and emittance of ~ 0.15–0.17. The coating was thermally stable up to 400 °C for 2 h in air. The selective property of the coating entirely lost ($\Delta\alpha$=−0.111 and $\Delta\varepsilon$=+0.05) after heat treatment at 425 °C in air due to diffusion of copper into the coating and formation of CuO. In order to enhance thermal stability, an additional Mo layer of thickness 40 nm was introduced on Cu substrate. The improvement in the thermal stability was reasonable after deposition of Mo layer as it acted as a diffusion barrier. The Mo/ $HfO_x/Mo/HfO_2$ coatings on both Cu and SS substrate were thermally stable up to 500 °C in air and 800 °C in vacuum. However, the coating degraded at 525 °C in air due to oxidation and phase transformation of Mo and formation of unwanted impurities such as MoO_2, MoO_3, and HfMo2O8.

6.8. $MgF_2/Mo/MgF_2$

In 1965, Schmidt and Park [206] prepared some interesting coating in different combinations of MgF_2, CeO_2 and Mo by electron beam evaporation techniques. The absorptance and emittance measurements were performed at 260 and 538 °C in vacuum. $MgF_2/Mo/MgF_2/Mo/MgF_2$ –based absorber coating on Mo substrate possesses high absorptance of 0.89 and low emittance of 0.075 while $MgF_2/Mo/CeO_2$ coating had absorptance and emittance of 0.85 and 0.053, respectively. A high absorptance of 0.85 and low emittance of 0.073 have been achieved by $MgF_2/CeO_2/Mo/MgF_2/CeO_2$ -based absorber coating. All the aforementioned absorptance and emittance value was collected at 260 °C in vacuum. At 538 °C, the emittance value for all these coatings increased while absorptance was constant. The emissivity of the coating increased slightly to 0.090 at 538 °C while the absorptance was constant.

Sergeant [53] modelled a DMD multilayer stack in very interesting way using the standard transfer matrix method where MgF_2 and TiO_2 with refractive index 1.37 and 2.75 at 1 μm respectively, served the function of dielectrics in the same coating, while Mo and W was used as the metal substrate as well as metallic layer, sandwiched between dielectrics. The combination of MgF_2 and TiO_2 was preferred as dielectric due to contrast in their refractive index (Δn =1.38; λ=1 μm) and high thermal resistance. Two sets of four DMD coatings made of Mo, MgF_2, TiO_2 and W, MgF_2, TiO_2 with no of layers =5,7,9,11 have been optimized at 720 K. The coating structures are presented in Fig. 21 and Fig. 22. The metal substrate W or Mo is counted as L =1. The optimized coating exhibited high solar absorptance (> 94%) in the wavelengths shorter than 2.24 μm, and low absorption (< 7%) in the wavelength beyond 2.24 μm which is shown by Fig. 23(a) and Fig. 23(b). They have also demonstrated that the merit function of the absorber coating (see Eq. (11)) increases with increasing the number of layers up to L=11, which is presented in Fig. 23(c). However, the performance saturates while the number of layers exceed than 11. If the number of layers is increased more than 11, an increase

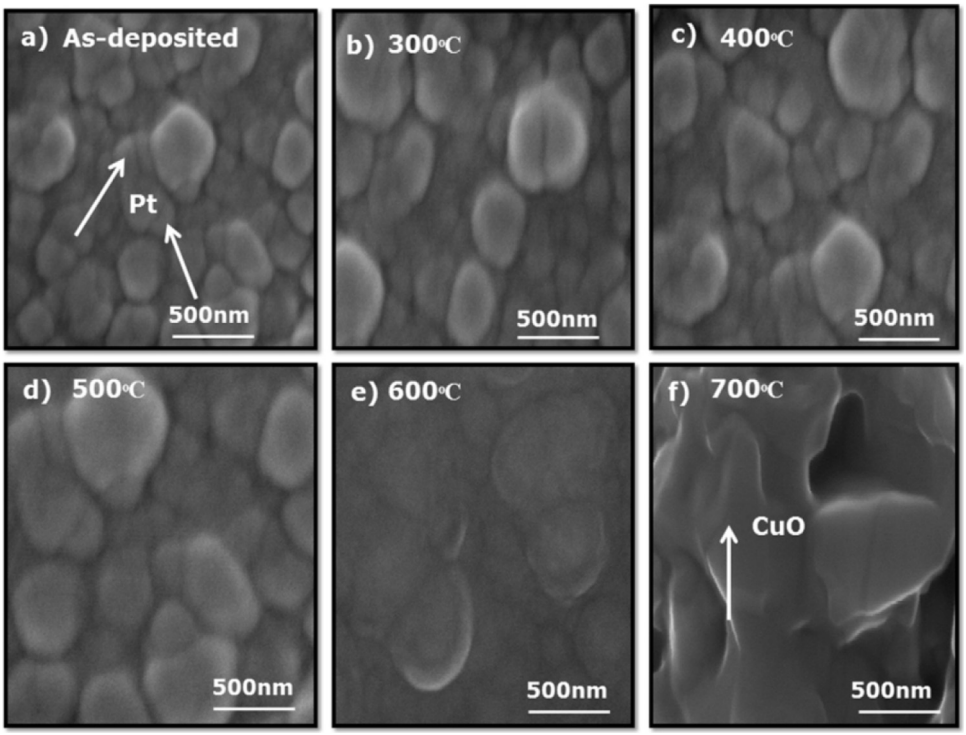

Fig. 17. SEM images of as deposited (a) and heat treated coatings in air at (b) 300 °C (c) 400 °C (d) 500 °C (e) 600 °C and (f) 700 °C of $Al_xO_y/Pt/Al_xO_y$ coating on Cu substrates [214].

in emittance has been observed due to thicker coating. The angular spectral selectivity of both the DMD absorbers have been studied and the coatings have a wide angular absorption. The wide angle absorption along with high selectivity and thermal stability indicates the coatings as a potential candidate for CSP applications.

We have attempted to give the reader an overview of the research findings on the DMD -based solar selective absorber coatings till date in detail. DMD-based absorber coatings show their significant potential as a different class of solar selective absorber coatings; their exceptional attraction lies on the thin film design with a combination of metal and dielectric layers. Tables (2–4) summarize the absorptance, emittance, short and long term thermal stability in air and vacuum of the DMD –based absorber coatings studied using different deposition techniques or modelling method. It can be commented that further advancements in DMD –based absorber coating can be made to obtain selectivity like an ideal solar selective absorber.

7. A way forward towards subwavelength texturing of DMD stack

So far we have discussed about different solar selective absorber coatings based on DMD configuration. Even though the coatings are extremely effective, a common feature of the top dielectric layers is their higher refractive index than air. Therefore, these materials in a planar form inevitably produce a strong, undesired loss of sunlight in

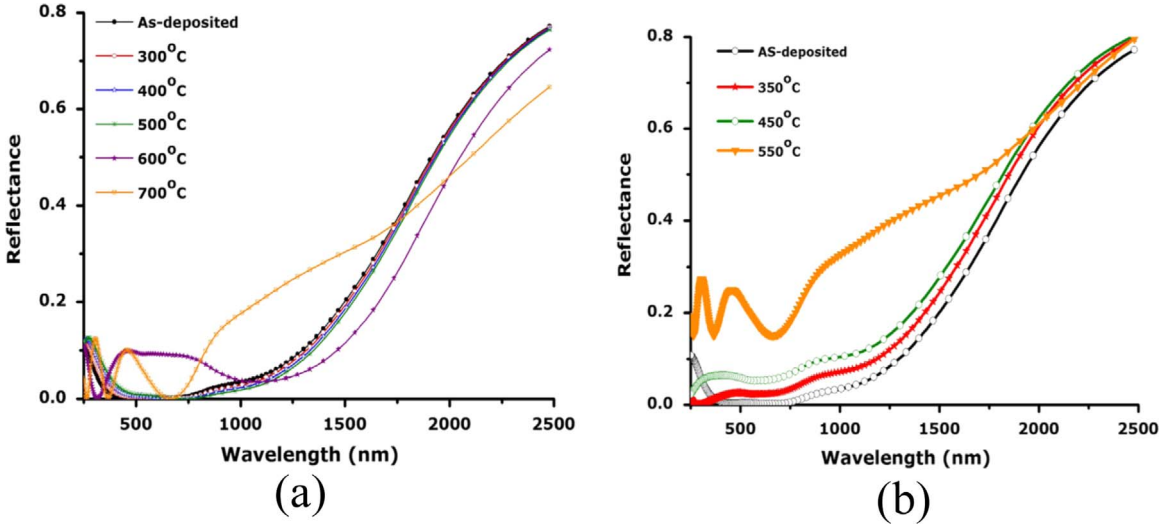

Fig. 18. Thermal stability study of $Al_xOy/Pt/Al_xO_y$ in different temperatures in air for (a) 2 h and (b) 24 h [214].

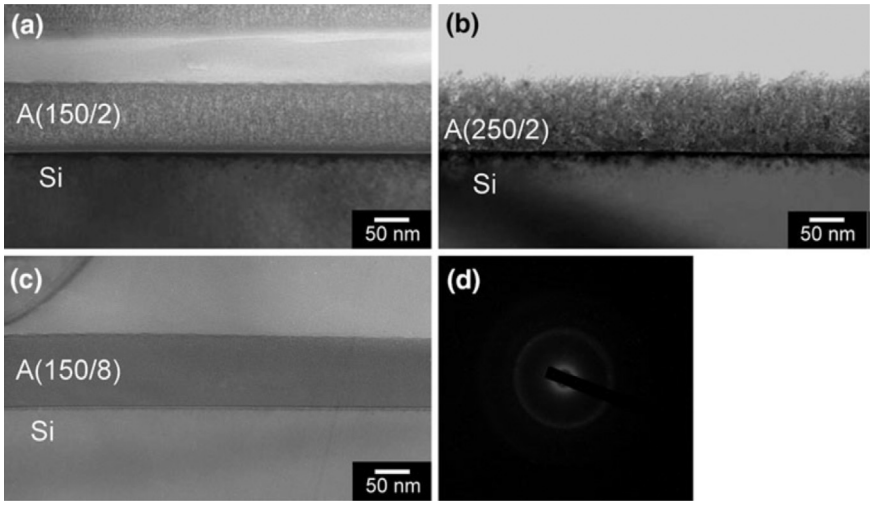

Fig. 19. TEM cross-sectional images of as-deposited coating Al_xO_y coatings deposited using different DC powers and oxygen flow rates; A (p/q) represents Al_xO_y coating (DC power/ oxygen flow rate) (a) A (150/2), (b) A (250/2) and (c) A (150/8) ; (d) diffraction pattern of as-deposited A (150/2)[217].

air/dielectric interface, because of Fresnel reflection [237]. Based on the strong light concentration and scattering properties, light-trapping layers employing metallic nanostructures have gained significant attention over the past decade [238,239]. It can be an interesting idea to combine the DMD stack with a proper light-trapping texture at a subwavelength scale on the dielectric surface to manipulate light absorption by suppressing Fresnel reflection over a wide range of wavelengths. The texturing of the surface may include V-shaped groove, nanowires, particles, voids, dual-diameter nanopillars, nanocones and domes, etc., which support strong optical resonances that can enhance and effectively control broad-band light absorption as well as scattering processes. In Fig. 24, we have shown a comparison between the flat surface with an ideal textured surface of 45°. The later configuration gives the incident light an opportunity to interact with the surface for a second time [237]. A careful engineering of the texture designs with proper size and shape will allow very strong optical resonances that can further boost light–matter interaction compared to flat surfaces [240]. This light trapping concept offers a great flexibility and tunability and can be extended for use in many other applications. The texturing of the surface have already enabled performance improvement in crystalline silicon (*c*-Si) solar cells and nanoscale optoelectronic devices [241,242]. With the advances in nanofabrication techniques over the past decade, such structures now can be synthesized by inexpensive, scalable deposition or wet-chemical etching techniques and can provide high efficiency at extremely low cost. It can be anticipated that the implementation of textured surface in DMD stack can spark a wave of new research aiming to reach the highest selective performance by utilizing the incident solar radiation more efficiently.

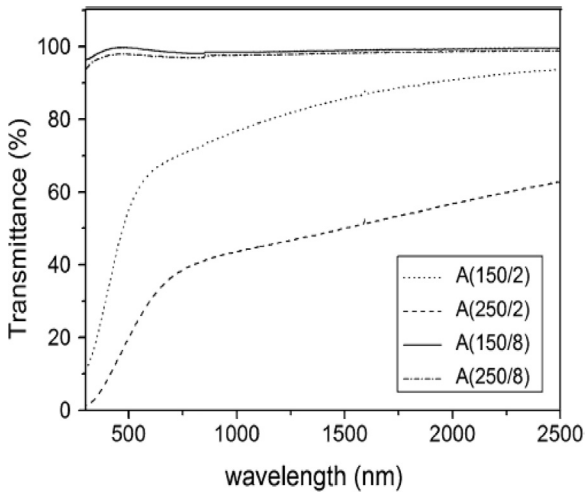

Fig. 20. Transmittance spectra of Al_xO_y fabricated in different taget power and oxygen gas flow rate. A(p/q) denotes Al_xO_y coating (DC power/ oxygen flow rate) [217].

8. Future perspective and recommendations

It is evident from the review that the research on solar selective absorber coating is a dynamic field, whose significance and industrial viability will undoubtedly progress in the future. The DMD -based absorber coatings have accomplished the desired selective property close to an ideal solar selective absorber coating as serious research has been conducted on it in recent decades.

The confinement of electromagnetic wave using a plasmonic geometry DMD stack introduces many advantages for the conversion of solar energy to thermal energy as well as the thermal stability of the coating. Researchers have exploited the ellipsomoetry measurements to identify the metallic or dielectric nature of individual layer of DMD – based solar selective absorber coatings. However, more attention should be paid theoretically and experimentally to explore the underlying physical mechanisms that govern the excellent selectivity of the coatings rather than demonstrating the metallic and dielectric properties. In fact, the in depth study will help to carefully design an absorber consisting of multiple numbers of periodic metal and dielectric layers. It has been reported that a dielectric layer with very high refractive index ($n_d > 2$) and a relatively thick metal layer can satisfy a “zero reflection condition”, i.e. highest absorptance [170]. Therefore, it is proposed to investigate the selection of proper combination of the metals and dielectrics to boost the absorptance properties.

Despite the fact that there are number of DMD -based absorber coatings, their practical applications in the actual field still remain a challenge and are liable to numerous other important properties. In this regard, it should be prime aim to concentrate on their corrosion resistance, scratch resistance, hardness, abrasion, hydrophobic nature and performance in humid environment. A year round performance assessment in different climatic conditions is required to prove reliability and weather proofing capability of the absorbers. While evaluating the annual performance and designing the operational strategy, one needs to take into account the variation of solar radiation in different time throughout the year.

The optical absorptance in DMD coating is enhanced due to the

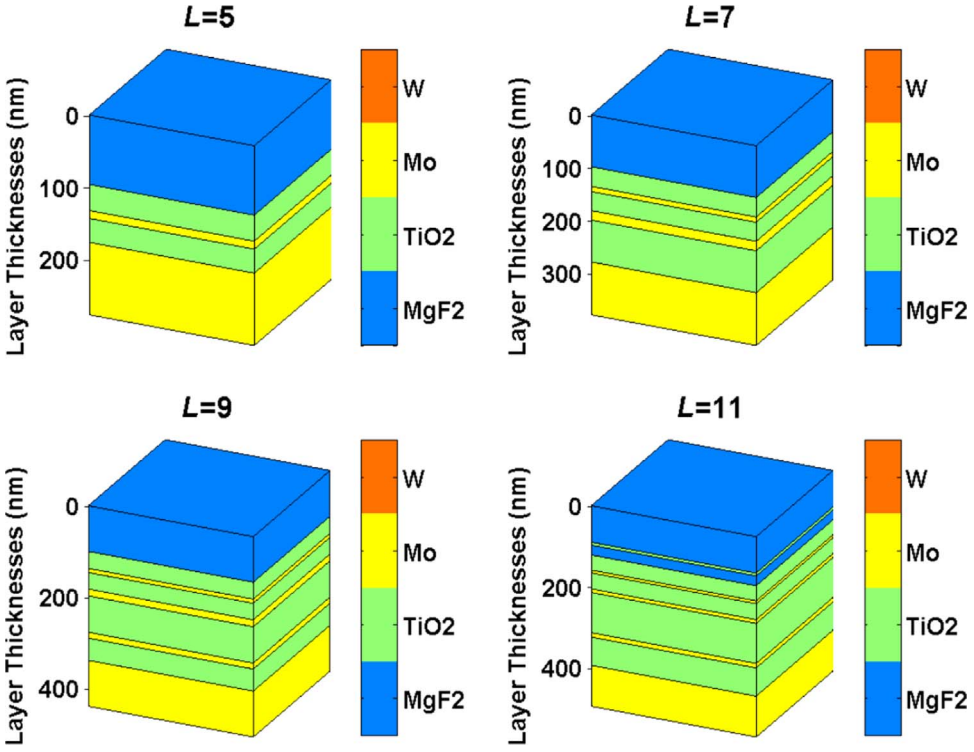

Fig. 21. Schematic of DMD coatings with Mo, MgF_2 and TiO_2 layers. Optimized stacks with no of layers L =5, 7, 9 and 11 are shown [53].

surface plasmon polaritons in the metal-dielectric interface. In order to boost the absorptance further, an intriguing approach could be to stack multiple metal dielectric layers in alternative way. It is essential to take into account optical constants of the metals and dielectric components of the multilayer DMD coating over a wide wavelength range. Furthermore, theoretical absorptance and emittance is needed to explore before starting experimental procedures.

To develop a highly efficient CSP system, it is also required to investigate how the incident angle of solar radiation can change the optical properties of the absorber coating [97]. The slight change in incident angle can introduce a large variation in optical thickness as well as phase difference between incident and reflected rays, which cause a noticeable difference in the reflectance spectra of absorber coating [170]. Hence, the sensitive angular dependence of the absorber coating should be unrevealed before practical application of it in CSP plants.

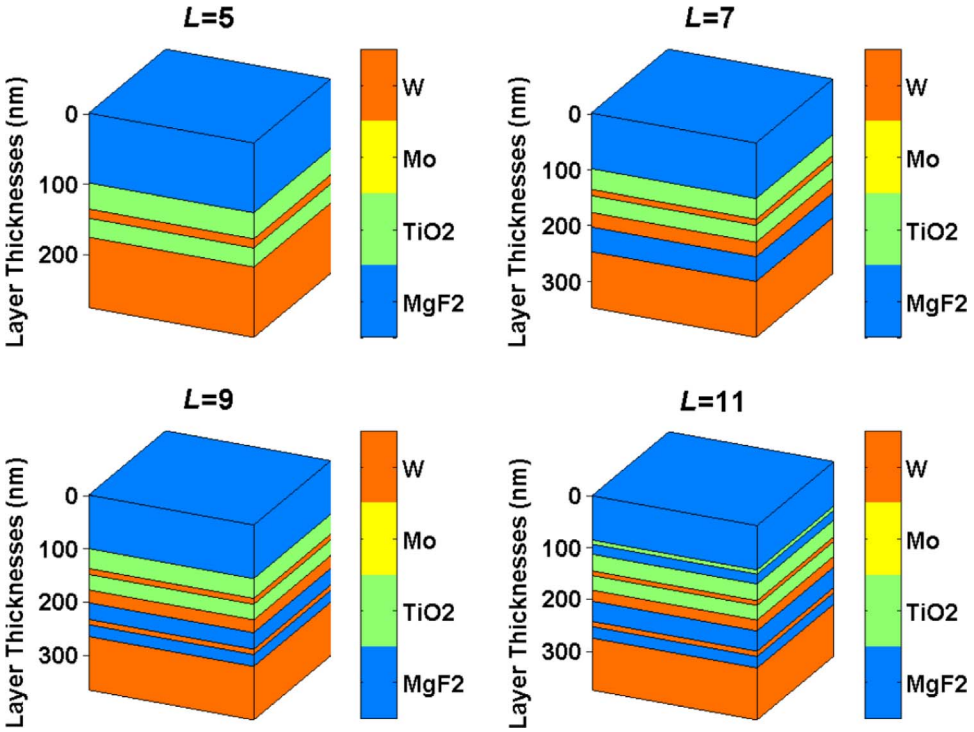

Fig. 22. Schematic of DMD coatings with W, MgF_2 and TiO_2 layers. Optimized stacks with no of layers L =5, 7, 9 and 11 are shown [53].

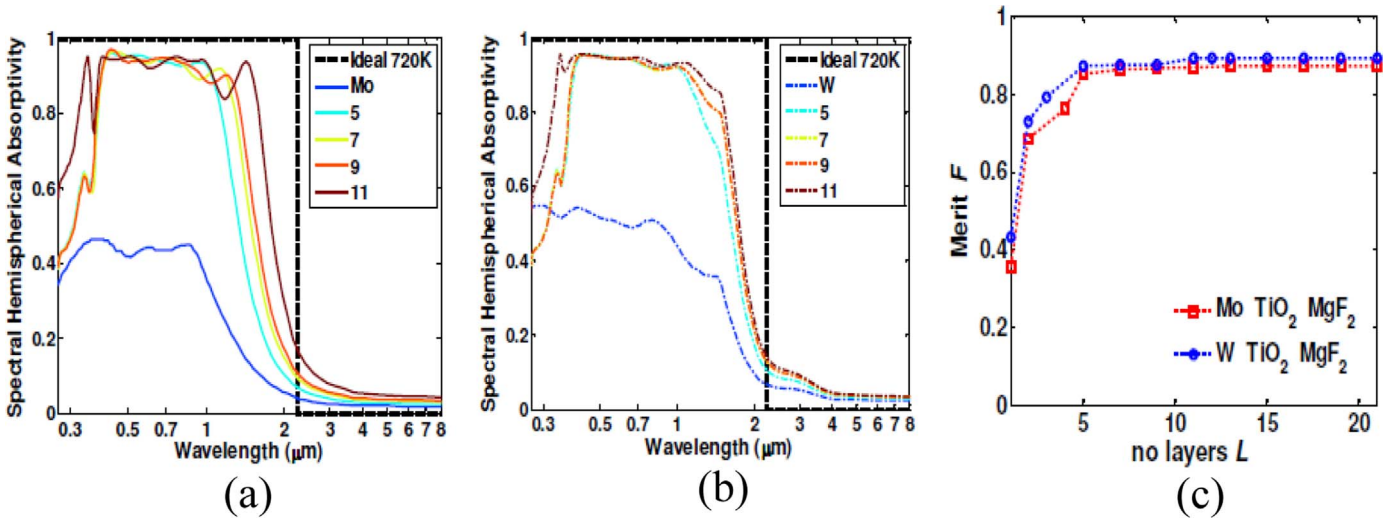

Fig. 23. Absorption spectra of the metal-dielectric stack composed of (a) Mo, TiO_2 and MgF_2 (b) W, TiO_2 and MgF_2. The spectra selectivity of ideal selective absorber at 720 K has also been plotted as reference (c) The variation of merit function of the metal-dielectric stack using Mo, TiO_2, MgF_2 and W, TiO_2, MgF_2. The substrate (Mo or W) has been considered as L =1 [53].

Table 2
Optical properties and thermal stability of dielectric-metal-dielectric (DMD) -based absorber coatings deposited by reactive DC magnetron sputtering.

Coatings	Substrate	Thickness (nm) (bottom to top)	Absorptance (α)	Emittance (ε)	Thermal stability				References
					Short-term (2 h)		Long term		
					air	vac	air	vac	
$Cr_xO_y/Cr/Cr_2O_3$	Cu	28 /13/ 64	0.899 – 0.912	0.05 – 0.06	300 °C	500 °C	250 °C, 250 hrs	-	[152]
$Al_xO_y/Al/Al_xO_y$	Cu, Mo	40/15/97	0.950 - 0.970	0.05 - 0.08	400 °C	800 °C	250 °C, 200 hrs 300 °C, 25 hrs	-	[149]
$Al_xO_y/Ni/Al_xO_y$	SS	70/20/70	0.932	0.038	-	-	400 °C, 12 hrs	-	[217]
$HfO_x/Mo/HfO_2$	Cu	26/31/67	0.905-0.923	0.07-0.09	400 °C	-	-	-	[153]
$Mo/HfO_x/Mo/HfO_2$	Cu	Mo interlayer ~ 40 nm	”	”	500 °C	800 °C			[153]
$HfO_x/Mo/HfO_2$	SS	-	0.902-0.917	0.15-0.17	-	-	-	-	[153]
$Mo/HfO_x/Mo/HfO_2$	SS	Mo interlayer ~ 40 nm	”	”	500 °C	-	800 °C	-	[153]

Table 3
Dielectric-metal-dielectric (DMD) -based solar selective absorber coatings fabricated by electron beam evaporation technique unless otherwise mentioned.

Coatings	Substrate	Thickness (nm) (bottom to top)	Absorptance (α)	Emittance (ε)	Thermal stability				References
					Short term		Long term		
					air (2 h)	vac	air (24 h)	vac	
MgO/Zr/MgO	Zr coated SS	78.3/10/92.6	0.92	0.09	300 °C	400 °C, 2 hrs	250 °C	-	[199, 200]
$Al_xO_y/Pt/Al_xO_y$	Cu	40/7/90	0.94 ± 0.01	0.06 ± 0.01	500 °C	-	450 °C	-	[212, 214]
Ta/ $Al_xO_y/Pt/Al_xO_y$	Cu	40/7/90	0.940	0.09	700 °C	-	550 °C	-	[209]
$MgF_2/Mo/CeO_2$	Mo	-	0.85	0.053 (260 °C), 0.062 (538 °C)	-	538 °C	-	-	[206]
$MgF_2/Mo/MgF_2/Mo/MgF_2$	Mo	-	0.89	0.075 (260 °C), 0.090 (538 °C)	-	538 °C	-	-	[206]
$MgF_2/CeO_2/Mo/MgF_2/CeO_2$	Mo	-	0.85	0.073 (260 °C), 0.084 (538 °C)	-	538 °C	-	-	[206]
$Al_2O_3/Mo/Al_2O_3/Mo/Al_2O_3/Mo/Al_2O_3/Mo$	Mo	-	0.91	0.085 (260 °C) 0.016 (538 °C)	-	538 °C	-	-	[206]
$Al_2O_3/Mo/Al_2O_3/Mo/Al_2O_3/Mo/Al_2O_3$	Mo		0.91	0.085 (260 °C), 0.16 (538 °C)	-	-	-	-	[206]
$Al_2O_3/Mo/Al_2O_3$*	Mo	Mo ~ 200 Å	0.85	0.11 (500 °C), 0.22 (1000 °C)	-	1050 °C, 1 hr	-	920 °C, 500 hrs	[207]
$Al_2O_3/Mo/Al_2O_3$*	Mo (3000 - 6000 Å) coated SS	Mo ~ 200 Å	-	-	-	900 °C, 1 hr	-	-	[207]

* Vacuum evaporation

Table 4
Optically modelled dielectric-metal-dielectric (DMD) -based solar selective absorber coatings using transfer matrix approach.

Coatings	Substrate	Absorptance (α)	Emittance (ε)	References
$Mo/TiO_2/MgF_2$ (No of layers: 11)	Mo	0.94	0.06 (447 °C)	[53]
$W/TiO_2/MgF_2$ (No of layers: 11)	W	0.95	0.06 (447 °C)	[53]

this issue, it is necessary to fabricate the DMD coatings by cost-effective wet chemistry route. However, it has been noted that wet chemistry route can produce high surface roughness, non-uniformity and defect on the coating, which result a low solar selective property [248]. Hence, many technical limitations need to overcome before developing potential DMD coating by cheap and moderately efficient wet-chemistry method as most of the coatings prepared by this techniques exhibit less selectivity and low thermal stability. Appropriate understanding on thin-film deposition procedures can help in accomplishing highly efficient selective coating, which can be demonstrated commercially in different CSP systems. To further promote and engineer new, exotic and more efficient coating structures, a number of approaches can be

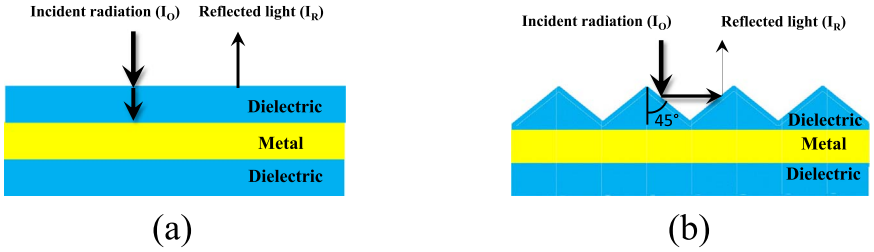

Fig. 24. The interaction of light with (a) flat and (b) textured DMD coatings [237].

In current research trend of developing solar selective materials, another issue is the high temperature stability, which is of extreme significance. The prolonged exposure under concentrated solar radiation is likely to provoke substrate-absorber layer inter diffusion, and consequently, modify layer interfaces, compositions and optical properties. Therefore, attractiveness lies in choosing the reliable materials which should yield high melting point and high activation energy for oxidation.

Another strategy is to introduce a metallic diffusion barrier in between the absorber coating and the substrate [243]. This layer hinders metal atoms from entering the absorber layer at high temperatures and prevents the change in optical properties of the coating. The substrate diffusion can also be restricted by pre-heat treatment of stainless steel in air before depositing any layer. In terms of long term durability under high temperature conditions, the single dielectric layer on top of the coating is vulnerable. Inclusion of another dense anti-reflection layer on top of the dielectric will protect the film by preventing oxidation from the surroundings [201]. Along with the anti-reflection properties, the top layer should have extremely high hardness and scratch resistance property [244,245], so that the entire stack can be handled easily.

Most published studies on DMD based coating were focused on new design concepts of the metal dielectric stack, investigation on optical properties and the thermal stability of the coating. However, none of the papers have mentioned the economic analysis or LCOE (levelized cost of electricity) [246] using these coatings. The lack of such important information would lead to uncertainty and confusion in the scientific community. It may also be an interesting approach to calculate the LCOC (levelized cost of coating) to compare the selectivity of different alternative coating as a function of durability. Therefore, it is of utmost importance to provide a possible description on cost analysis which may be helpful for initial commercialization of the film.

It is also worth noting that although the magnetron sputtering technique is exceptionally attractive for fabricating DMD coating, the essential problem of this method is the high cost due to the advanced system and energy consumption. There should be an optimum balance between efficiency, durability, high temperature stability, costs and the manufacture procedure for large scale applications [247]. To address pursued by utilizing the basic principles of physics and chemistry.

It is also exceptionally fascinating to study which deposition technique or which absorber structure will at last succeed commercially. However, it would unquestionably be dictated by the straightforwardness of manufacturability and expense of the power per watt. The DMD –based solar selective coatings can also be utilised in a proficient thermo-photovoltaic system, an integrated system combining a solar photovoltaic and solar thermal panel. In such systems, the DMD-based absorber will confine the sun rays, heat up, and emit towards a solar cell a narrow-banded spectrum directly above the band-gap of the solar cell.

In summary, it will be interesting to perceive how the performance and applications of DMD-based absorber coatings evolve in terms of cost, reliability of the materials, testing requirements, market strength, and most importantly the constant demand on renewable energy along with enormous research effort to make the CSP system competitive with the conventional power generation. It can be anticipated that the combined efforts into the further progress on fabrication procedures, structure and material optimization, energy conversion and effectiveness, performance testing will have significant impact in developing superior DMD -based absorber coatings.

9. Conclusions

In this review paper, we have made an attempt to discuss various types of solar selective absorber coatings including intrinsic absorbers, semiconductor absorbers, multilayer absorbers, cermets or metal-dielectric absorbers, textured surface, with emphasis on dielectric – metal – dielectric absorbers (DMD). Undoubtedly DMD -based coatings represent a promising approach in energy conversion from abundant solar energy to thermal energy. From our perspective, the beneficial effects associated with SPP have proven DMD stack as universal and versatile plasmonic structure to concentrate the entire solar spectrum and to meet the growing demand of low-cost, environment friendly solar energy. The DMD absorbers cover a vast number of materials from different metals (Cr, Zr, Mo, Al, Pt, Ni) to dielectrics (Cr_2O_3, MgO, Al_2O_3, HfO_2, MgF_2), thereby offer a wide variety of choices in terms of the optical properties. Such adaptability permits

customizing and designing the coating as well as aims at enhancing the spectral performance. As far as high temperature stability is concerned, some crucial changes are needed to acquire the desired performances of the coatings. Therefore, we anticipate that increasing number of studies on DMD-based coating are needed as there is adequate room for designing industrially accessible specific coatings. Furthermore, we believe that this review will bridge the literature gap on DMD -based solar absorber coatings and point a way towards the future of renewable energy.

Acknowledgements

This paper is based upon work supported in part under the US-India Partnership to Advance Clean Energy-Research (PACE-R) for the Solar Energy Research Institute for India and the United States (SERIIUS), funded jointly by the U.S. Department of Energy (Office of Science, Office of Basic Energy Sciences, and Energy Efficiency and Renewable Energy, Solar Energy Technology Program, under Subcontract DE-AC36-08GO28308 to the National Renewable Energy Laboratory, Golden, Colorado) and the Government of India, through the Department of Science and Technology under Subcontract IUSSTF/JCERDC-SERIIUS/2012 dated 22nd Nov. 2012. Atasi Dan thanks DST for providing INSPIRE scholarship. She also thanks SERIIUS-Mageep fellowship for their financial support to visit WashU.

Appendix A

List of symbols

Symbol	Definition
α	solar absorptance
ε	thermal emittance
λ	wavelength
$G_{\lambda,abs}$	absorbed radiation
G_{λ}	incident radiation
$E_{b\lambda}$	radiant energy from a black body
c	speed of light
h	Planck's constant
k_B	Boltzmann's constant
T	temperature
σ	Stefan-Boltzmann constant
E_g	band gap
$\eta_{sol-the}$	solar to thermal conversion efficiency
C_{annual}	total annualized coating costs
$E_{thermal}$	average annual energy absorbed
C	solar concentration ratio
I	solar flux density
ε^{MG}	average dielectric functions of the composite in MG approximations
ε^{BR}	average dielectric functions of the composite in BR approximations
ε_A	dielectric function of metal
ε_B	dielectric function of ceramic
f_A	volume fraction occupied by metal
μ	combined density of state mass
$E_v(k)$	energy of valance band
$E_c(k)$	energy of conductance band
$P_{cv}(\mathbf{k})$	momentum matrix element between valance and conduction band states
E_O	peak transition energy
A_L	strength of the transition
C_L	broadening of the transition
n	refractive index
k	extinction co-efficient
ε_M	complex dielectric constant of metal
ε_∞	high-frequency component of the dielectric constant
ω_p	plasma frequency
Γ_D	damping factor
d	diameter of nano particle
Q	Joule losses in metal
E	electric field
E_m	electric field in metal
E_d	electric field in dielectric
k_x	wavevector parallel to the interface
k_z,m	perpendicular to the interface in the metal
k_z,d	perpendicular to the interface in dielectric

k_{SP}	wave vector (momentum) of the SPPs
k_o	wave vector (momentum) of the photon
$P_{abs,d}$	power absorbed by the dielectric
$P_{abs,m}$	power absorbed by the metal
F_{abs}	ratio of dissipative power in metal and dielectric
tanδ	Loss factor
ε'	real part of the relative permittivity
ε''	imaginary part of the relative permittivity
$\overline{\delta_r}$	phase thickness
$\overline{\eta_r}$	complex admittance in the horizontal and vertical directions
ρ(r, ω)	local density of optical states
hω	photon energy
k_BT	thermal energy
η_d	real part of the refractive index of dielectric
η_m	real part of the refractive index of metal
k_d	imaginary part of the refractive index of dielectric
k_m	imaginary part of the refractive index of metal
R	universal gas constant

List of acronyms

CSP	Concentrating Solar Power
SPP	Surface Plasma Polariton
DMD	Dielectric-Metal-Dielectric
MD	Metal-Dielectric
TES	Thermal Energy Storage
BS	Backup Systems
IEA	International Energy Agency
ESTELA	European Solar Thermal Electricity Association
JNNSM	Jawaharlal Nehru National Solar Mission
LCOC	Levelized Cost of Coating
PVD	Physical Vapour Deposition
EM	Electromagnetic
UHTCs	Ultra-High Temperature Ceramics
FDTD	Finite-Difference Time Domain
AR	Anti reflection
MG	Maxwell-Garnett
BR	Bruggeman
HMVF	High Metal Volume Fraction
LMVF	Low Metal Volume Fraction
PhC	Photonic Crystal
RCWA	Rigorous Coupled-Wave Analysis
LSP	Localised Surface Plasmon
TM	Transverse-Magnetic
XPS	X-ray photoelectron spectroscopy
XRD	X-ray diffraction
SEM	Scanning Electron microscopy
DC	Direct Current
RF	Radio Frequency
PC	Performance criterion function
LCOE	Levelized Cost of Electricity

References

[1] Unruh GC. Escaping carbon lock-in. Energy Policy 2002;30:317–25.
[2] Gupta PK. Renewable energy sources—a longway to go in India. Renew Energy 1999;16:1216–9.
[3] Athienitis AK, Santamouris M. Thermal analysis and design of passive solar buildings. Earthscan, 711 Third Avenue, New York, NY 10017: Routledge; 2013.
[4] Kalkan N, Dagtekin I. Passive solar techniques to improve thermal comfort and reduce energy consumption of domestic use. World Acad Sci Eng Technol Int J Electr Comput Energ Electron Commun Eng 2016;10:432–7.
[5] Mazarrón FR, Porras-Prieto CJ, García JL, Benavente RM. Feasibility of active solar water heating systems with evacuated tube collector at different operational water temperatures. Energy Convers Manag 2016;113:16–26.
[6] Singh DB, Yadav JK, Dwivedi VK, Kumar S, Tiwari GN, Al-Helal IM. Experimental studies of active solar still integrated with two hybrid PVT collectors. Sol Energy 2016;130:207–23.
[7] Chow TT. A review on photovoltaic/thermal hybrid solar technology. Appl Energy 2010;87:365–79.
[8] Price H, Kearney D Reducing the cost of energy from parabolic trough solar power plants. American Society of Mechanical Engineers. p. 591–599.
[9] Zhang HL, Baeyens J, Degrève J, Cacères G. Concentrated solar power plants: review and design methodology. Renew Sustain Energy Rev 2013;22:466–81.
[10] OECD/IEA, technology roadmap, concentrating solar power. 2010.
[11] Lotker M. Barriers to commercialization of large-scale solar electricity: lessions learned from the LUZ experience. Albuquerque, NM (United States): Sandia National Labs.; 1991.
[12] Osuna R, Fernandez V, Romero M, Marcos MJ. PS10, A 10 MW Solar Tower Power Plant for Southern Spain; 2001.
[13] Fthenakis V, Mason JE, Zweibel K. The technical, geographical, and economic

feasibility for solar energy to supply the energy needs of the US. Energy Policy 2009;37:387–99.
[14] Pitz-Paa R, Amin A, Oliver Bettzuge M, et al. Concentrating Solar Power in Europe, the Middle East and North Africa: A Review of Development Issues and Potential to 2050. ASME. J. Sol. Energy Eng. 2012;134(2):024501–6. http://dx.doi.org/10.1115/1.4006390.
[15] Purohit I, Purohit P. Techno-economic evaluation of concentrating solar power generation in India. Energy Policy 2010;38:3015–29.
[16] Hang Q, Jun Z, Xiao Y, Junkui C. Prospect of concentrating solar power in China—the sustainable future. Renew Sustain Energy Rev 2008;12:2505–14.
[17] Müller-Steinhagen H, Trieb F. Concentrating solar power. A review of the technology Ingenia. Inform QR Acad Eng 2004;18:43–50.
[18] Trieb F, Müller-Steinhagen H. Concentrating solar power for seawater desalination in the Middle East and North Africa. Desalination 2008;220:165–83.
[19] Fluri TP. The potential of concentrating solar power in South Africa. Energy Policy 2009;37:5075–80.
[20] Hinkley JT, Hayward JA, Curtin B, Wonhas A, Boyd R, Grima C, et al. An analysis of the costs and opportunities for concentrating solar power in Australia. Renew Energy 2013;57:653–61.
[21] Abbas M, Boumeddane B, Said N, Chikouche A. Dish Stirling technology: a 100 MW solar power plant using hydrogen for Algeria. Int J Hydrog Energy 2011;36:4305–14.
[22] Cau G, Cocco D. Comparison of medium-size concentrating solar power plants based on parabolic trough and linear Fresnel collectors. Energy Procedia 2014;45:101–10.
[23] Romero M, González-Aguilar J. Solar thermal CSP technology. Wiley Interdiscip Rev: Energy Environ 2014;3:42–59.
[24] Ummadisingu A, Soni MS. Concentrating solar power–technology, potential and policy in India. Renew Sustain Energy Rev 2011;15:5169–75.
[25] Kuravi S, Trahan J, Goswami DY, Rahman MM, Stefanakos EK. Thermal energy storage technologies and systems for concentrating solar power plants. Prog Energy Combust Sci 2013;39:285–319.
[26] Barlev D, Vidu R, Stroeve P. Innovation in concentrated solar power. Sol Energy Mater Sol Cells 2011;95:2703–25.
[27] Alex S, Chattopadhyay K, Basu B. Tailored specular reflectance properties of bulk Cu based novel intermetallic alloys. Sol Energy Mater Sol Cells 2016;149:66–74.
[28] Alex S, Basu B, Sengupta S, Pandey UK, Chattopadhyay K. Electrodeposition of δ-phase based Cu-Sn mirror alloy from sulfate-aqueous electrolyte for solar reflector application. Appl Therm Eng 2016.
[29] Chen CJ. Physics of solar energy. John Wiley & Sons; 2011.
[30] Skiff FA. Solar heater. Google Patents; 1913.
[31] Anderson WA. Solar heating element. Google Patents; 1926.
[32] Miller KW. Solar heat trap. Google Patents; 1954.
[33] Zvi TH. Receiver for solar energy collectors. Google Patents; 1959.
[34] Barshilia HC, Selvakumar N, Rajam KS, Rao DVS, Muraleedharan K. Deposition and characterization of TiAlN/TiAlON/Si_3N_4 tandem absorbers prepared using reactive direct current magnetron sputtering. Thin Solid Films 2008;516:6071–8.
[35] Choy KL. Chemical vapour deposition of coatings. Prog Mater Sci 2003;48:57–170.
[36] Alami AH, Allagui A, Alawadhi H. Synthesis and optical properties of electrodeposited crystalline Cu_2O in the Vis–NIR range for solar selective absorbers. Renew Energy 2015;82:21–5.
[37] Kaluža L, Orel B, Dražič G, Kohl M. Sol–gel derived $CuCoMnO_x$ spinel coatings for solar absorbers: structural and optical properties. Sol Energy Mater Sol Cells 2001;70:187–201.
[38] Orel ZC, Gunde MK. Spectrally selective paint coatings: preparation and characterization. Sol Energy Mater Sol Cells 2001;68:337–53.
[39] Bogaerts WF, Lampert CM. Materials for photothermal solar energy conversion. J Mater Sci 1983;18:2847–75.
[40] Niklasson GA, Granqvist CG. Surfaces for selective absorption of solar energy: an annotated bibliography 1955–1981. J Mater Sci 1983;18:3475–534.
[41] Kennedy CE. Review of mid-to high-temperature solar selective absorber materials. Golden, Colo, USA: National Renewable Energy Laboratory; 2002.
[42] Granqvist CG. Solar energy materials. Adv Mater 2003;15:1789–803.
[43] Gadgil SB, Thangaraj R, Iyer JV, Sharma AK, Gupta BK, Agnihotri OP. Spectrally selective copper sulphide coatings. Sol Energy Mater 1981;5:129–40.
[44] Granqvist CG, Wittwer V. Materials for solar energy conversion: an overview. Sol Energy Mater Sol Cells 1998;54:39–48.
[45] Wijewardane S, Goswami DY. A review on surface control of thermal radiation by paints and coatings for new energy applications. Renew Sustain Energy Rev 2012;16:1863–73.
[46] Amri A, Jiang ZT, Pryor T, Yin C-Y, Djordjevic S. Developments in the synthesis of flat plate solar selective absorber materials via sol–gel methods: a review. Renew Sustain Energy Rev 2014;36:316–28.
[47] Atkinson C, Sansom CL, Almond HJ, Shaw CP. Coatings for concentrating solar systems–a review. Renew Sustain Energy Rev 2015;45:113–22.
[48] Jeeva SN PA, Karthikeyan S. A review on Black coatings for Solar Energy Storaging Systems. Int J ChemTech Res 2016;9(03):589–96.
[49] Selvakumar N, Barshilia HC. Review of physical vapor deposited (PVD) spectrally selective coatings for mid-and high-temperature solar thermal applications. Sol Energy Mater Sol Cells 2012;98:1–23.
[50] Jackson JD. Classical electrodynamics. Classical electrodynamics: Wiley; 1999.
[51] Kuhn TS. Black-body theory and the quantum discontinuity. Chicago and London: University of Chicago Press; 1978. p. 1894–912.
[52] Cardy J. The ubiquitous 'c': from the Stefan–Boltzmann law to quantum information Boltzmann Medal Lecture, Statphys24, Cairns, July 2010. J Stat Mech: Theory Exp 2010;2010:P10004.
[53] Sergeant NP, Pincon O, Agrawal M, Peumans P. Design of wide-angle solar-selective absorbers using aperiodic metal-dielectric stacks. Opt Express 2009;17:22800–12.
[54] Cindrella L. The real utility ranges of the solar selective coatings. Sol Energy Mater Sol Cells 2007;91:1898–901.
[55] Ho CK, Mahoney AR, Ambrosini A, Bencomo M, Hall A, Lambert TN Characterization of Pyromark 2500 for high-temperature solar receivers. American Society of Mechanical Engineers. p. 509–518.
[56] Bermel P, Lee J, Joannopoulos JD, Celanovic I, Soljacie M. Selective solar absorbers. Annu Rev Heat Transf 2012:15.
[57] Li P, Liu B, Ni Y, Liew KK, Sze J, Chen S, et al. Large-scale nanophotonic solar selective absorbers for high-efficiency solar thermal energy conversion. Adv Mater 2015;27:4585–91.
[58] Ho CK, Pacheco JE. Levelized Cost of Coating (LCOC) for selective absorber materials. Sol Energy 2014;108:315–21.
[59] Ehrenreich H, Seraphin BO. Symposium on the Fundamental Optical Properties of Solids Relevant to Solar Energy Conversion. NASA STI/Recon Technical Report N;77:12538; 1975.
[60] Touloukian YS, Powell RW, Ho CY, Nicolaou MC. Thermophysical properties of matter-the TPRC data series. Therm Diffus DTIC Doc 1974;10.
[61] González F, Barrera-Calva E, Huerta L, Mane RS. Coatings of Fe_3O_4 nanoparticles as selective solar absorber. Open Surf Sci J 2011;3:131–5.
[62] Ienei E, Isac L, Duta A. Synthesis of alumina thin films by spray pyrolysis. Rev Roum Chim 2010;55:161–5.
[63] Randich E, Allred DD. Chemically vapor-deposited ZrB_2 as a selective solar absorber. Thin Solid Films 1981;83:393–8.
[64] Sani E, Mercatelli L, Sansoni P, Silvestroni L, Sciti D. Spectrally selective ultra-high temperature ceramic absorbers for high-temperature solar plants. J Renew Sustain Energy 2012;4:033104.
[65] Sani E, Mercatelli L, Francini F, Sans JL, Sciti D. Ultra-refractory ceramics for high-temperature solar absorbers. Scr Mater 2011;65:775–8.
[66] Shah AA, Ungaro C, Gupta MC. High temperature spectral selective coatings for solar thermal systems by laser sintering. Sol Energy Mater Sol Cells 2015;134:209–14.
[67] Chen Z, Boström T. Anti-reflection coated spectrally selective carbon nanotube solar absorbers. Renew Energy Environ Sustain 2016;1:2.
[68] Chen Z, Boström T. Electrophoretically deposited carbon nanotube spectrally selective solar absorbers. Sol Energy Mater Sol Cells 2016;144:678–83.
[69] Ding D, Cai W, Long M, Wu H, Wu Y. Optical, structural and thermal characteristics of Cu–$CuAl_2O_4$ hybrids deposited in anodic aluminum oxide as selective solar absorber. Sol Energy Mater Sol Cells 2010;94:1578–81.
[70] Geng QF, Zhao X, Gao XH, Liu G. Sol–gel combustion-derived $CoCuMnO_x$ spinels as pigment for spectrally selective paints. J Am Ceram Soc 2011;94:827–32.
[71] Pal S, Diso D, Franza S, Licciulli A, Rizzo L. Spectrally selective absorber coating from transition metal complex for efficient photothermal conversion. J Mater Sci 2013;48:8268–76.
[72] Jerman I, Mihelčič M, Verhovšek D, Kovač J, Orel B. Polyhedral oligomeric silsesquioxane trisilanols as pigment surface modifiers for fluoropolymer based Thickness Sensitive Spectrally Selective (TSSS) paint coatings. Sol Energy Mater Sol Cells 2011;95:423–31.
[73] Geng Q, Zhao X, Gao X, Yu H, Yang S, Liu G. Optimization design of $CuCr_xMn_{2-x}O_4$-based paint coatings used for solar selective applications. Sol Energy Mater Sol Cells 2012;105:293–301.
[74] Geng Q, Zhao X, Gao X, Yang S, Liu G. Low-temperature combustion synthesis of $CuCr_2O_4$ spinel powder for spectrally selective paints. J Sol-Gel Sci Technol 2012;61:281–8.
[75] Ambrosini A, Lambert TN, Bencomo M, Hall A, Siegel NP, Ho CK Improved high temperature solar absorbers for use in concentrating solar power central receiver applications. American Society of Mechanical Engineers. p. 587-594.
[76] Orel ZC, Gunde MK, Hutchins MG. Spectrally selective solar absorbers in different non-black colours. Sol Energy Mater Sol Cells 2005;85:41–50.
[77] Paone A, Geiger M, Sanjines R, Schüler A. Thermal solar collector with VO_2 absorber coating and $V_{1-x}W_xO_2$ thermochromic glazing–temperature matching and triggering. Sol Energy 2014;110:151–9.
[78] Sciti D, Silvestroni L, Trucchi DM, Cappelli E, Orlando S, Sani E. Femtosecond laser treatments to tailor the optical properties of hafnium carbide for solar applications. Sol Energy Mater Sol Cells 2015;132:460–6.
[79] Fang Z, Lu C, Guo C, Lu Y, Gao D, Ni Y, et al. Suitability of layered Ti_3SiC_2 and $Zr_3[Al(Si)]_4C_6$ ceramics as high temperature solar absorbers for solar energy applications. Sol Energy Mater Sol Cells 2015;134:252–60.
[80] Xiaohong XU, Zhenggang RAO, Jianfeng WU, Yonghua LI, Zhang Y, Xinbin LAO. In-situ synthesis and thermal shock resistance of cordierite/silicon carbide composites used for solar absorber coating. Sol Energy Mater Sol Cells 2014;130:257–63.
[81] Agnihotri OP, Gupta BK. Solar selective surfaces; 1981.
[82] Moon J, Lu D, VanSaders B, Kim TK, Kong SD, Jin S, et al. High performance multi-scaled nanostructured spectrally selective coating for concentrating solar power. Nano Energy 2014;8:238–46.
[83] Yang L, Mo L, Chen T, Forsberg E, He S. A checkerboard selective absorber with excellent spectral selectivity. J Appl Phys 2015;118:183103.
[84] Wang KK, Wu ZZ, Peng CJ, Wang KP, Cheng B, Song CL, et al. A facile process to prepare crosslinked nano-graphites uniformly dispersed in titanium oxide films as solar selective absorbers. Sol Energy Mater Sol Cells 2015;143:198–204.
[85] Kuckelkorn T, Graf W. Radiation-selective absorber coating with an adherent oxide layer and method of making same. Google Patents; 2010.

[86] Richards BS. Comparison of TiO_2 and other dielectric coatings for buried-contact solar cells: a review. Prog Photovolt: Res Appl 2004;12:253–81.
[87] Seraphin BO. Chemical vapor deposition of thin semiconductor films for solar energy conversion. Thin Solid Films 1976;39:87–94.
[88] Selvakumar N, Barshilia HC, Rajam KS, Biswas A. Spectrally selective TiAlN/CrAlON/Si_3N_4 tandem absorber for high temperature solar applications; 2008.
[89] Zou C, Xie W, Shao L. Functional multi-layer solar spectral selective absorbing coatings of AlCrSiN/AlCrSiON/AlCrO for high temperature applications. Sol Energy Mater Sol Cells 2016;153:9–17.
[90] Rebouta L, Capela P, Andritschky M, Matilainen A, Santilli P, Pischow K, et al. Characterization of TiAlSiN/TiAlSiON/SiO_2 optical stack designed by modelling calculations for solar selective applications. Sol Energy Mater Sol Cells 2012;105:202–7.
[91] Selvakumar N, Manikandanath NT, Biswas A, Barshilia HC. Design and fabrication of highly thermally stable HfMoN/HfON/Al_2O_3 tandem absorber for solar thermal power generation applications. Sol Energy Mater Sol Cells 2012;102:86–92.
[92] Liu HD, Fu TR, Duan MH, Wan Q, Chen YM, Fu DJ, et al. Structure and thermal stability of spectrally selective absorber based on AlCrON coating for solar-thermal conversion applications. Sol Energy Mater Sol Cells 2016;157:108–16.
[93] Eisenhammer T, Haugeneder A, Mahr A. High-temperature optical properties and stability of selective absorbers based on quasicrystalline AlCuFe. Sol Energy Mater Sol Cells 1998;54:379–86.
[94] Hao L, Du M, Liu X, Wang S, Jiang L, Lü F, et al. Thermal stability of nitride solar selective absorbing coatings used in high temperature parabolic trough current. Sci China Technol Sci 2010;53:1507–12.
[95] Du M, Hao L, Mi J, Lv F, Liu X, Jiang L, et al. Optimization design of $Ti_{0.5}Al_{0.5}N$/$Ti_{0.25}Al_{0.75}N$/AlN coating used for solar selective applications. Sol Energy Mater Sol Cells 2011;95:1193–6.
[96] Valleti K, Krishna DM, Joshi SV. Functional multi-layer nitride coatings for high temperature solar selective applications. Sol Energy Mater Sol Cells 2014;121:14–21.
[97] Dan A, Chattopadhyay K, Barshilia HC, Basu B. Angular solar absorptance and thermal stability of W/WAlN/WAlON/Al_2O_3-based solar selective absorber coating. Appl Therm Eng 2016.
[98] Dan A, Jyothi J, Chattopadhyay K, Barshilia HC, Basu B. Spectrally selective absorber coating of WAlN/WAlON/Al_2O_3 for solar thermal applications. Sol Energy Mater Sol Cells 2016;157:716–26.
[99] Dan A, Chattopadhyay K, Barshilia HC, Basu B. Colored selective absorber coating with excellent durability. Thin Solid Films 2016;620:17–22.
[100] Zettl M. High performance coatings for solar receivers and new dedicated manufacturing solution. Energy Procedia 2014;48:701–6.
[101] ALMECO Group SBoT. ⟨http://www.almecogroup.com/en/pagina/16-solar⟩; 2014.
[102] Bayón R, San Vicente G, Morales Á. Durability tests and up-scaling of selective absorbers based on copper–manganese oxide deposited by dip-coating. Sol Energy Mater Sol Cells 2010;94:998–1004.
[103] Joly M, Antonetti Y, Python M, Gonzalez M, Gascou T, Scartezzini J-L, et al. Novel black selective coating for tubular solar absorbers based on a sol–gel method. Sol Energy 2013;94:233–9.
[104] Khan MR, Wang X, Alam MA. Fundamentals of PV efficiency: limits for light absorption. arXiv Prepr arXiv 2012;12122897.
[105] Berini P. Long-range surface plasmon polaritons. Adv Opt Photonics 2009;1:484–588.
[106] Green MA, Pillai S. Harnessing plasmonics for solar cells. Nat Photonics 2012;6:130–2.
[107] Garnett JCM. Colours in metal glasses, in metallic films, and in metallic solutions. II. Philos Trans R Soc Lond Ser A, Contain Pap A Math Or Phys Character 1906:237–88.
[108] Bruggeman VDAG. Berechnung verschiedener physikalischer Konstanten von heterogenen Substanzen. I. Dielektrizitätskonstanten und Leitfähigkeiten der Mischkörper aus isotropen Substanzen. Ann Phys 1935;416:636–64.
[109] Craighead HG, Howard RE, Sweeney JE, Buhrman RA. Graded-index Pt-Al_2O_3 composite solar absorbers. Appl Phys Lett 1981;39:29–31.
[110] Fan JCC, Spura SA. Selective black absorbers using rf-sputtered Cr2O3/Cr cermet films. Appl Phys Lett 1977;30:511–3.
[111] Kumar SN, Malhotra LK, Chopra KL. Nickel pigmented anodized aluminium as solar selective absorbers. Sol Energy Mater 1983;7:439–52.
[112] Zhang Q-C. Stainless-steel–AlN cermet selective surfaces deposited by direct current magnetron sputtering technology. Sol Energy Mater Sol Cells 1998;52:95–106.
[113] Cespedes E, Wirz M, Sánchez-García JA, Alvarez-Fraga L, Escobar-Galindo R, Prieto C. Novel Mo–Si_3N_4 based selective coating for high temperature concentrating solar power applications. Sol Energy Mater Sol Cells 2014;122:217–25.
[114] Antonaia A, Castaldo A, Addonizio ML, Esposito S. Stability of W-Al_2O_3 cermet based solar coating for receiver tube operating at high temperature. Sol Energy Mater Sol Cells 2010;94:1604–11.
[115] Xue Y, Wang C, Wang W, Liu Y, Wu Y, Ning Y, et al. Spectral properties and thermal stability of solar selective absorbing AlNi–Al_2O_3 cermet coating. Sol Energy 2013;96:113–8.
[116] Barshilia HC, Kumar P, Rajam KS, Biswas A. Structure and optical properties of Ag–Al_2O_3 nanocermet solar selective coatings prepared using unbalanced magnetron sputtering. Sol Energy Mater Sol Cells 2011;95:1707–15.
[117] Nuru ZY, Arendse CJ, Nemutudi R, Nemraoui O, Maaza M. Pt–Al_2O_3 nanocoatings for high temperature concentrated solar thermal power applications. Phys B: Condens Matter 2012;407:1634–7.
[118] Xinkang D, Cong W, Tianmin W, Long Z, Buliang C, Ning R. Microstructure and spectral selectivity of Mo–Al_2O_3 solar selective absorbing coatings after annealing. Thin Solid Films 2008;516:3971–7.
[119] Wang J, Wei B, Wei Q, Li D. Optical property and thermal stability of Mo/Mo–SiO_2/SiO_2 solar-selective coating prepared by magnetron sputtering. Phys Status Solidi (a) 2011;208:664–7.
[120] Zheng L, Zhou F, Zhou Z, Song X, Dong G, Wang M, et al. Angular solar absorptance and thermal stability of Mo–SiO_2 double cermet solar selective absorber coating. Sol Energy 2015;115:341–6.
[121] Adsten M, Joerger R, Järrendahl K, Wäckelgård E. Optical characterization of industrially sputtered nickel–nickel oxide solar selective surface. Sol Energy 2000;68:325–8.
[122] Cao F, Kraemer D, Tang L, Li Y, Litvinchuk AP, Bao J, et al. A high-performance spectrally-selective solar absorber based on a yttria-stabilized zirconia cermet with high-temperature stability. Energy Environ Sci 2015;8:3040–8.
[123] Zhang Q-C, Yin Y, Mills DR. High efficiency Mo·Al_2O_3 cermet selective surfaces for high-temperature application. Sol Energy Mater Sol Cells 1996;40:43–53.
[124] Zhang Q-C, Mills D, Monger A. Thin film solar selective surface coating. Google Patents; 1996.
[125] Esposito S, Antonaia A, Addonizio ML, Aprea S. Fabrication and optimisation of highly efficient cermet-based spectrally selective coatings for high operating temperature. Thin Solid Films 2009;517:6000–6.
[126] Zhang Q-C. Metal-AlN cermet solar selective coatings deposited by direct current magnetron sputtering technology. J Phys D: Appl Phys 1998;31:355.
[127] Wang X, Li H, Yu X, Shi X, Liu J. High-performance solution-processed plasmonic Ni nanochain-Al_2O_3 selective solar thermal absorbers. Appl Phys Lett 2012;101:203109.
[128] Katumba G, Makiwa G, Baisitse TR, Olumekor L, Forbes A, Wäckelgård E. Solar selective absorber functionality of carbon nanoparticles embedded in SiO_2. ZnO NiO Matrices Phys Status Solidi (C) 2008;5:549–51.
[129] Katumba G, Olumekor L, Forbes A, Makiwa G, Mwakikunga B, Lu J, et al. Optical, thermal and structural characteristics of carbon nanoparticles embedded in ZnO and NiO as selective solar absorbers. Sol Energy Mater Sol Cells 2008;92:1285–92.
[130] Roro KT, Tile N, Mwakikunga B, Yalisi B, Forbes A. Solar absorption and thermal emission properties of multiwall carbon nanotube/nickel oxide nanocomposite thin films synthesized by sol–gel process. Mater Sci Eng: B 2012;177:581–7.
[131] Cuevas A, Martinez L, Romero R, Dalchiele EA, Marotti R, Leinen D, et al. Electrochemically grown cobalt-alumina composite layer for solar thermal selective absorbers. Sol Energy Mater Sol Cells 2014;130:380–6.
[132] Cao F, McEnaney K, Chen G, Ren Z. A review of cermet-based spectrally selective solar absorbers. Energy Environ Sci 2014;7:1615–27.
[133] Konttinen P, Lund PD, Kilpi RJ. Mechanically manufactured selective solar absorber surfaces. Sol Energy Mater Sol Cells 2003;79:273–83.
[134] Konttinen P, Kilpi R, Lund PD. Microstructural analysis of selective C/Al_2O_3/Al solar absorber surfaces. Thin Solid Films 2003;425:24–30.
[135] Chen J, Ye H, Ae L, Tang Y, Kieven D, Rissom T, et al. Tapered aluminum-doped vertical zinc oxide nanorod arrays as light coupling layer for solar energy applications. Sol Energy Mater Sol Cells 2011;95:1437–40.
[136] Kumar SK, Suresh S, Murugesan S, Raj SP. CuO thin films made of nanofibers for solar selective absorber applications. Sol Energy 2013;94:299–304.
[137] Sergeant NP, Agrawal M, Peumans P. High performance solar-selective absorbers using coated sub-wavelength gratings. Opt Express 2010;18:5525–40.
[138] Joannopoulos JD, Johnson SG, Winn JN, Meade RD. Photonic crystals: molding the flow of light. New Jersey: Princeton University Press; 2011.
[139] Wang J, Chen Z, Li D. Simulation of two-dimensional Mo photonic crystal surface for high-temperature solar-selective absorber. Phys Status Solidi (a) 2010;207:1988–92.
[140] Wang H, Sivan VP, Mitchell A, Rosengarten G, Phelan P, Wang L. Highly efficient selective metamaterial absorber for high-temperature solar thermal energy harvesting. Sol Energy Mater Sol Cells 2015;137:235–42.
[141] Barnes WL, Dereux A, Ebbesen TW. Surface plasmon subwavelength optics. Nature 2003;424:824–30.
[142] Zayats AV, Smolyaninov II, Maradudin AA. Nano-optics of surface plasmon polaritons. Phys Rep 2005;408:131–314.
[143] von Blanckenhagen B, Tonova D, Ullmann J. Application of the Tauc-Lorentz formulation to the interband absorption of optical coating materials. Appl Opt 2002;41:3137–41.
[144] Adachi S. Optical dispersion relations for Si and Ge. J Appl Phys 1989;66:3224–31.
[145] Kreibig U, Vollmer M. Optical properties of metal clusters. New York: Springer Science & Business Media; 2013.
[146] Ninomiya S, Adachi S. Optical properties of wurtzite CdS. J Appl Phys 1995;78:1183–90.
[147] Adachi S, Mori H, Ozaki S. Model dielectric function for amorphous semiconductors. Phys Rev B 2002;66:153201.
[148] Jellison GE, Jr, Modine FA. Parameterization of the optical functions of amorphous materials in the interband region. Appl Phys Lett 1996;69:371–3.
[149] Barshilia HC, Selvakumar N, Vignesh G, Rajam KS, Biswas A. Optical properties and thermal stability of pulsed-sputter-deposited AlxOy/Al/AlxOy multilayer absorber coatings. Sol Energy Mater Sol Cells 2009;93:315–23.
[150] Sahoo NK, Thakur S, Senthilkumar M, Bhattacharyya D, Das NC. Reactive electron beam evaporation of gadolinium oxide optical thin films for ultraviolet and deep ultraviolet laser wavelengths. Thin Solid Films 2003;440:155–68.
[151] Wooten F. Optical properties of solids. New York, USA: Academic Press; 2013.
[152] Barshilia HC, Selvakumar N, Rajam KS, Biswas A. Structure and optical properties

of pulsed sputter deposited Cr_xO_y/ Cr/ Cr_2O_3 solar selective coatings. J Appl Phys 2008;103:023507.
[153] Selvakumar N, Barshilia HC, Rajam KS, Biswas A. Structure, optical properties and thermal stability of pulsed sputter deposited high temperature HfO_x/Mo/ HfO_2 solar selective absorbers. Sol Energy Mater Sol Cells 2010;94:1412–20.
[154] Ritchie RH. Plasma losses by fast electrons in thin films. Phys Rev 1957;106:874.
[155] Powell CJ, Swan JB. Origin of the characteristic electron energy losses in aluminum. Phys Rev 1959;115:869.
[156] Stern EA, Ferrell RA. Surface plasma oscillations of a degenerate electron gas. Phys Rev 1960;120:130.
[157] Hutter E, Fendler JH. Exploitation of localized surface plasmon resonance. Adv Mater 2004;16:1685–706.
[158] Stockman MI. Slow propagation, anomalous absorption, and total external reflection of surface plasmon polaritons in nanolayer systems. Nano Lett 2006;6:2604–8.
[159] Baba A, Advincula RC, Knoll W. In situ investigations on the electrochemical polymerization and properties of polyaniline thin films by surface plasmon optical techniques. J Phys Chem B 2002;106:1581–7.
[160] Brongersma ML, Kik PG. Surface plasmon nanophotonics. Netherlands: Springer; 2007.
[161] Kabashin AV, Evans P, Pastkovsky S, Hendren W, Wurtz GA, Atkinson R, et al. Plasmonic nanorod metamaterials for biosensing. Nat Mater 2009;8:867–71.
[162] Boltasseva A, Nikolajsen T, Leosson K, Kjaer K, Larsen MS, Bozhevolnyi SI. Integrated optical components utilizing long-range surface plasmon polaritons. J Light Technol 2005;23:413.
[163] Kawata S. Near-field microscope probes utilizing surface plasmon polaritons. Near-Field Opt Surf Plasmon Polaritons: Springe 2001:15–27.
[164] Homola J, Yee SS, Gauglitz G. Surface plasmon resonance sensors: review. Sens Actuators B: Chem 1999;54:3–15.
[165] Oulton RF, Sorger VJ, Zentgraf T, Ma R-M, Gladden C, Dai L, et al. Plasmon lasers at deep subwavelength scale. Nature 2009;461:629–32.
[166] Hobson PA, Wedge S, Wasey JAE, Sage I, Barnes WL. Surface plasmon mediated emission from organic light-emitting diodes. Adv Mater 2002;14:1393–6.
[167] Krokhin AA. Long-range surface plasmons in dielectric-metal-dielectric structure with highly anisotropic substrates. Phys Rev B 2010;81:085426.
[168] Bohn CD, Agrawal A, Lee Y, Choi CJ, Davis MS, Haney PM, et al. Design considerations for enhancing absorption in semiconductors on metals through surface plasmon polaritons. Phys Chem Chem Phys 2014;16:6084–91.
[169] Koev ST, Agrawal A, Lezec HJ, Aksyuk VA. An efficient large-area grating coupler for surface plasmon polaritons. Plasmonics 2012;7:269–77.
[170] Kim S, Lee J-L. Design of dielectric/metal/dielectric transparent electrodes for flexible electronics. J Photonics Energy 2012;2, [021215-].
[171] Kasap SO. Principles of electronic materials and devices. McGraw-Hill; 2006.
[172] Maier SA. Surface plasmon polaritons at metal/insulator interfaces. Plasmon: Fundam Appl 2007:21–37.
[173] Liddell HM, Jerrard HG. Computer-aided techniques for the design of multilayer filters. Bristol, UK: IOP Publishing Ltd; 1981.
[174] Liu X, Cai X, Qiao J, Mao J, Jiang N. The design of ZnS/Ag/ZnS transparent conductive multilayer films. Thin Solid Films 2003;441:200–6.
[175] Palik ED. Handbook of optical constants of solids. Academic Press; 1998.
[176] Johnson PB, Christy RW. Optical constants of the noble metals. Phys Rev B 1972;6:4370.
[177] Ramakrishna SA, Armour AD. Propagating and evanescent waves in absorbing media. Am J Phys 2003;71:562–7.
[178] Gibot P, Vidal L. Original synthesis of chromium (III) oxide nanoparticles. J Eur Ceram Soc 2010;30:911–5.
[179] Kim D-W, Shin S-I, Lee J-D, Oh S-G. Preparation of chromia nanoparticles by precipitation–gelation reaction. Mater Lett 2004;58:1894–8.
[180] Dube DC, Agrawal D, Agrawal S, Roy R. High temperature dielectric study of Cr2O3 in microwave region. Appl Phys Lett 2007;90:124105–9900.
[181] Sahoo S, Petracic O, Binek C, Kleemann W, Sousa JB, Cardoso S, et al. Superspin-glass nature of discontinuous Co 80 Fe 20/Al 2 O 3 multilayers. Phys Rev B 2002;65:134406.
[182] Sahoo S, Binek C. Piezomagnetism in epitaxial Cr_2O_3 thin films and spintronic applications. Philos Mag Lett 2007;87:259–68.
[183] Thongkanluang T, Kittiauchawal T, Limsuwan P. Preparation and characterization of Cr 2 O 3–TiO 2–Al 2 O 3–V 2 O 5 green pigment. Ceram Int 2011;37:543–8.
[184] Berdahl P. Pigments to reflect the infrared radiation from fire. J Heat Transf 1995;117:355–8.
[185] Khamlich S, McCrindle R, Nuru ZY, Cingo N, Maaza M. Annealing effect on the structural and optical properties of Cr/α-Cr 2 O 3 monodispersed particles based solar absorbers. Appl Surf Sci 2013;265:745–9.
[186] Teixeira V, Sousa E, Costa MF, Nunes C, Rosa L, Carvalho MJ, et al. Chromium-based thin sputtered composite coatings for solar thermal collectors. Vacuum 2002;64:299–305.
[187] Gall D, Gampp R, Lang HP, Oelhafen P. Pulsed plasma deposition of chromium oxide/chromium-cermet coatings. J Vac Sci Technol A 1996;14:374–9.
[188] Barshilia HC, Rajam KS. Reactive sputtering of hard nitride coatings using asymmetric-bipolar pulsed DC generator. Surf Coat Technol 2006;201:1827–35.
[189] Lampert CM. Thermal degradation of a black chrome solar selective absorber coating: short term. Lawrence Berkeley National Laboratory; 2011.
[190] Survilienė S, Češūnienė A, Juškėnas R, Selskienė A, Bučinskienė D, Kalinauskas P, et al. The use of trivalent chromium bath to obtain a solar selective black chromium coating. Appl Surf Sci 2014;305:492–7.
[191] Benedetti S, Benia H-M, Nilius N, Valeri S, Freund H-J. Morphology and optical properties of MgO thin films on Mo (001). Chem Phys Lett 2006;430:330–5.
[192] Kingery WD, Francl J, Coble RL, Vasilos T. Thermal conductivity: X, Data for several pure oxide materials corrected to zero porosity. J Am Ceram Soc 1954;37:107–10.
[193] Skvortsova V, Trinkler L The optical properties of magnesium oxide containing transition metal ions and defects produced by fast neutron irradiation. World Scientific and Engineering Academy and Society (WSEAS). p. 150–154.
[194] Tsang KL, Chen Y. Suppression of dielectric breakdown in MgO crystals at high temperatures by impurity doping. J Appl Phys 1983;54:4531–5.
[195] Charles E, Lorival R, Boyer A, Malbrunot P. A fast-response high-temperature high-pressure surface thermocouple. Sens Actuators 1984;6:135–42.
[196] Joo MH, Park KH, Lee JW. In-situ characterization of MgO surface with discharge aging at elevated temperatures of AC-plasma display panels. J Surf Anal 2008;14:412–5.
[197] Shih I, Wu SL, Li L, Qiu CX, Grant P, Denhoff MW. Effects of heat treatment on a MgOSi structure: a possible buffer layer structure for high-Tc superconductors. Mater Lett 1991;11:161–3.
[198] Maziere-Bezes D, Valignat J. Optical properties of gold-magnesia selective cermets. Sol Energy Mater 1982;7:203–11.
[199] Nuru ZY, Msimanga M, Muller TFG, Arendse CJ, Mtshali C. Maaza M. Microstructural, optical properties and thermal stability of MgO/Zr/MgO multi-layered selective solar absorber coatings. Sol Energy 2015;111:357–63.
[200] Nuru ZY, Perez D, Kaviyarasu K, Vantomme A, Maaza M. Annealing effect on the optical properties and interdiffusion of MgO/Zr/MgO multilayered selective solar absorber coatings. Sol Energy 2015;120:123–30.
[201] Boström TK, Wäckelgård E, Westin G. Anti-reflection coatings for solution-chemically derived nickel—alumina solar absorbers. Sol Energy Mater Sol Cells 2004;84:183–91.
[202] Woods BW, Thompson DW, Woollam JA. Gold-alumina cermet photothermal films. Thin Solid Films 2004;469:31–7.
[203] Niklasson GA, Granqvist CG. Optical properties and solar selectivity of coevaporated Co-Al_2O_3 composite films. J Appl Phys 1984;55:3382–410.
[204] Sella C, Kaba A, Berthier S, Lafait J. Low cost selective absorber based on a Fe-Al_2O_3 cermet film. Sol Energy Mater 1987;16:143–54.
[205] Lafait J, Berthier S, Sella C, Vien TK. Pt-Al_2O_3 selective absorber coatings for photothermal conversion up to 600 °C. Vacuum 1986;36:125–7.
[206] Schmidt RN, Park KC. High-temperature space-stable selective solar absorber coatings. Appl Opt 1965;4:917–25.
[207] Peterson RE, Ramsey JW. Thin film coatings in solar – thermal power systems. J Vac Sci Technol 1975;12:174–81.
[208] Thornton JA, Penfold AS, Lamb JL. Sputter-deposited Al_2O_3/Mo/Al_2O_3 selective absorber coatings. Thin Solid Films 1980;72:101–10.
[209] Nuru ZY, Arendse CJ, Khamlich S, Kotsedi L, Maaza M. A tantalum diffusion barrier layer to improve the thermal stability of Al_xO_y/Pt/Al_xO_y multilayer solar absorber. Sol Energy 2014;107:89–96.
[210] Usmani B, Vijay V, Chhibber R, Dixit A. Optimization of sputtered zirconium thin films as an infrared reflector for use in spectrally-selective solar absorbers. Thin Solid Films 2017;627:17–25.
[211] Thornton JA, Lamb JL. Thermal stability studies of sputter-deposited multilayer selective absorber coatings. Thin Solid Films 1982;96:175–83.
[212] Nuru ZY, Arendse CJ, Khamlich S, Maaza M. Optimization of Al_xO_y/Pt/Al_xO_y multilayer spectrally selective coatings for solar–thermal applications. Vacuum 2012;86:2129–35.
[213] Nuru ZY, Arendse CJ, Muller TFG, Maaza M. Structural and optical properties of Al_xO_y/Pt/Al_xO_y multilayer absorber. Mater Sci Eng: B 2012;177:1194–9.
[214] Nuru ZY, Arendse CJ, Muller TF, Khamlich S, Maaza M. Thermal stability of electron beam evaporated Al_xO_y/Pt/Al_xO_y multilayer solar absorber coatings. Sol Energy Mater Sol Cells 2014;120:473–80.
[215] Nuru ZY, Msimanga M, Arendse CJ, Maaza M. Heavy ion elastic recoil detection analysis of Al_xO_y/Pt/Al_xO_y multilayer selective solar absorber. Appl Surf Sci 2014;298:176–81.
[216] Nuru ZY, Arendse CJ, Mongwaketsi N, Gohshal SK, Nkosi M, Maaza M. Effects of substrate temperatures on the thermal stability of Al_xO_y/Pt/Al_xO_y multilayered selective solar absorber coatings. Renew Energy 2015;75:590–7.
[217] Tsai TK, Hsueh SJ, Fang JS. Optical properties of Al_xO_y/Ni/Al_xO_y multilayered absorber coatings prepared by reactive DC magnetron sputtering. J Electron Mater 2014;43:229–35.
[218] Tsai P-H, Chang-Liao K-S, Liu C-Y, Wang T-K, Tzeng PJ, Lin CH, et al. Novel SONOS-type nonvolatile memory device with optimal Al doping in HfAlO charge-trapping layer. IEEE Electron Device Lett 2008;29:265–8.
[219] Kingon AI, Maria J-P, Streiffer SK. Alternative dielectrics to silicon dioxide for memory and logic devices. Nature 2000;406:1032–8.
[220] Singh J, Wolfe DE, Miller RA, Eldridge JI, Zhu D-M. Tailored microstructure of zirconia and hafnia-based thermal barrier coatings with low thermal conductivity and high hemispherical reflectance by EB-PVD. J Mater Sci 2004;39:1975–85.
[221] Wang Y, Zhao Y, Shao J, Fan Z. Effect of native defects and laser-induced defects on multi-shot laser-induced damage in multilayer mirrors. Chin Opt Lett 2011;9:093102.
[222] Liu ZS, Tibuleac S, Shin D, Young PP, Magnusson R. High-efficiency guided-mode resonance filter. Opt Lett 1998;23:1556–8.
[223] Vargas M, Murphy NR, Ramana CV. Structure and optical properties of nanocrystalline hafnium oxide thin films. Opt Mater 2014;37:621–8.
[224] Jena S, Tokas RB, Misal JS, Rao KD, Udupa DV, Thakur S, et al. Effect of O_2/Ar gas flow ratio on the optical properties and mechanical stress of sputtered HfO_2 thin films. Thin Solid Films 2015;592:135–42.
[225] Jain RK, Gautam YK, Dave V, Chawla AK, Chandra R. A study on structural, optical and hydrophobic properties of oblique angle sputter deposited HfO_2 films.

Appl Surf Sci 2013;283:332–8.
[226] Lin S-S, Li H-R. The optical properties of hydrophilic Hf-doped HfO_2 nanoceramic films. Ceram Int 2013;39:7677–83.
[227] Vlček J, Belosludtsev A, Rezek J, Houška J, Čapek J, Čerstvý R, et al. High-rate reactive high-power impulse magnetron sputtering of hard and optically transparent HfO_2 films. Surf Coat Technol 2016;290:58–64.
[228] Vargas M, Murphy NR, Ramana CV. Tailoring the index of refraction of nanocrystalline hafnium oxide thin films. Appl Phys Lett 2014;104:101907.
[229] Wang J, Li HP, Stevens R. Hafnia and hafnia-toughened ceramics. J Mater Sci 1992;27:5397–430.
[230] Liu W, Su X-p, Zhang S-y, Wang H-b, Hao P. Preparation and properties of hafnium oxide protective films on ZnS substrates. Laser Infrared 2007;8:021.
[231] Fadel M, Omer OA, Basily RR. A study of some optical properties of hafnium dioxide (HfO_2) thin films and their applications. Appl Phys A 1998;66:335–43.
[232] Torchio P, Gatto A, Alvisi M, Albrand G, Kaiser N, Amra C. High-reflectivity HfO_2/SiO_2 ultraviolet mirrors. Appl Opt 2002;41:3256–61.
[233] Khoshman JM, Khan A, Kordesch ME. Amorphous hafnium oxide thin films for antireflection optical coatings. Surf Coat Technol 2008;;202:2500–2.
[234] Al-Kuhaili MF. Optical properties of hafnium oxide thin films and their application in energy-efficient windows. Opt Mater 2004;27:383–7.
[235] Lesser M. Antireflection coatings for silicon charge-coupled devices. Opt Eng 1987;26, 269911-.
[236] Jain RK, Gautam YK, Dave V, Chawla AK, Chandra R. A study on structural, optical and hydrophobic properties of oblique angle sputter deposited HfO 2 films. Appl Surf Sci 2013;283:332–8.
[237] Sai H, Matsui T, Saito K, Kondo M, Yoshida I. Photocurrent enhancement in thin-film silicon solar cells by combination of anti-reflective sub-wavelength structures and light-trapping textures. Prog Photovolt: Res Appl 2015;23:1572–80.
[238] Ferry VE, Sweatlock LA, Pacifici D, Atwater HA. Plasmonic nanostructure design for efficient light coupling into solar cells. Nano Lett 2008;8:4391–7.
[239] Collin S, Pardo F, Teissier R, Pelouard J-L. Efficient light absorption in metal–semiconductor–metal nanostructures. Appl Phys Lett 2004;85:194–6.
[240] Brongersma ML, Cui Y, Fan S. Light management for photovoltaics using high-index nanostructures. Nat Mater 2014;13:451–60.
[241] Grandidier J, Weitekamp RA, Deceglie MG, Callahan DM, Battaglia C, Bukowsky CR, et al. Solar cell efficiency enhancement via light trapping in printable resonant dielectric nanosphere arrays. Phys Status Solidi (a) 2013;210:255–60.
[242] Lee Y-J, Ruby DS, Peters DW, McKenzie BB, Hsu JWP. ZnO nanostructures as efficient antireflection layers in solar cells. Nano Lett 2008;8:1501–5.
[243] Sibin KP, John S, Barshilia HC. Control of thermal emittance of stainless steel using sputtered tungsten thin films for solar thermal power applications. Sol Energy Mater Sol Cells 2015;133:1–7.
[244] Yin Y, Hang L, Zhang S, Bui XL. Thermal oxidation properties of titanium nitride and titanium–aluminum nitride materials—a perspective for high temperature air-stable solar selective absorber applications. Thin Solid Films 2007;515:2829–32.
[245] Roos A, Georgson M. Tin-oxide-coated anodized aluminium selective absorber surfaces II. Aging and durability. Sol Energy Mater 1991;22:29–41.
[246] Branker K, Pathak MJM, Pearce JM. A review of solar photovoltaic levelized cost of electricity. Renew Sustain Energy Rev 2011;15:4470–82.
[247] Wäckelgård E, Hultmark G. Industrially sputtered solar absorber surface. Sol Energy Mater Sol Cells 1998;54:165–70.
[248] Vince J, Vuk AŠ, Krašovec UO, Orel B, Köhl M, Heck M. Solar absorber coatings based on CoCuMnO x spinels prepared via the sol–gel process: structural and optical properties. Sol Energy Mater Sol Cells 2003;79:313–30.